ORIGINAL RESEARCH

Physico-chemical and pro-wound healing properties of microporous cellulosic sponge from *Gleditsia triacanthos* pods functionalized with *Phytolacca americana* fruit extract

Ioana Cristina Marinas · Gratiela Gradisteanu Pircalabioru · Eliza Oprea ·
Elisabeta-Irina Geana · Irina Zgura · Cosmin Romanitan · Elena Matei · Marian Angheloiu ·
Oana Brincoveanu · Mihaela Georgescu · Mariana Carmen Chifiriuc

Abstract This study aimed to exploit two invasive plant species to develop a novel, multifunctional, bioactive wound dressing based on a microporous cellulosic sponge (CS) from *Gleditsia triacanthos* pods and functionalizing them with *Phytolacca americana* fruit extract. The CS was functionalized, lyophilized, and characterized by Attenuated total reflectance–Fourier transform infrared spectroscopy, X-ray diffraction, scanning electron microscopy, contact angle, water absorption, and retention capacity. In addition, two parameters were evaluated in temporal dynamics: controlled release of phenolic compounds and antioxidant activities. The hemolytic index, blood clotting kinetics, lactate dehydrogenase release, and wound scratch assays proved their hemo- and biocompatibility, as well as their ability to promote cell proliferation and migration promoting-activity and to inhibit microbial growth. Furthermore, the obtained spongious material exhibited an anti-inflammatory effect by modulating the macrophages' secretion profile of IL-6 and IL-10. In conclusion, the microporous cellulosic sponge obtained from *G. triacanthos* could

Ioana C. Marinas and Gratiela Gradisteanu Pircalabioru have contributed equally.

Supplementary Information The online version contains supplementary material available at https://doi.org/10.1007/s10570-023-05491-3.

I. C. Marinas · G. Gradisteanu Pircalabioru ·
O. Brincoveanu · M. Georgescu · M. C. Chifiriuc
Research Institute of the University of Bucharest—ICUB, University of Bucharest, 050095 Bucharest, Romania

I. C. Marinas · M. Angheloiu
Research and Development Department of SC Sanimed International Impex SRL, 6 Bucharest-Giurgiu Street, 087040 Giurgiu, Romania

G. Gradisteanu Pircalabioru
Romanian Academy of Scientists, 54 Spl. Independenței St., District 5, 50085 Bucharest, Romania

E. Oprea (✉) · M. C. Chifiriuc
Department of Botany and Microbiology, Faculty of Biology, University of Bucharest, 1-3 Portocalelor Street, 060101 Bucharest, Romania
e-mail: eliza.oprea@g.unibuc.ro

E.-I. Geana
National R&D Institute for Cryogenics and Isotopic Technologies—ICSI Rm. Valcea, 4 Uzinei Street, PO Raureni, 240050 Ramnicu Valcea, Romania

I. Zgura · E. Matei
National Institute of Materials Physics, 405A Atomistilor Street, 077125 Magurele, Romania

C. Romanitan · O. Brincoveanu
National Institute for Research and Development in Microtechnologies IMT-Bucharest, 126A Erou Iancu Nicolae Street, 077190 Bucharest, Romania

M. C. Chifiriuc
The Romanian Academy, 25, Calea Victoriei, Sector 1, District 1, 010071 Bucharest, Romania

be used as a vehicle to ensure the controlled release of bioactive principles with pro-wound healing activities extracted from invasive plants.

Graphical abstract:
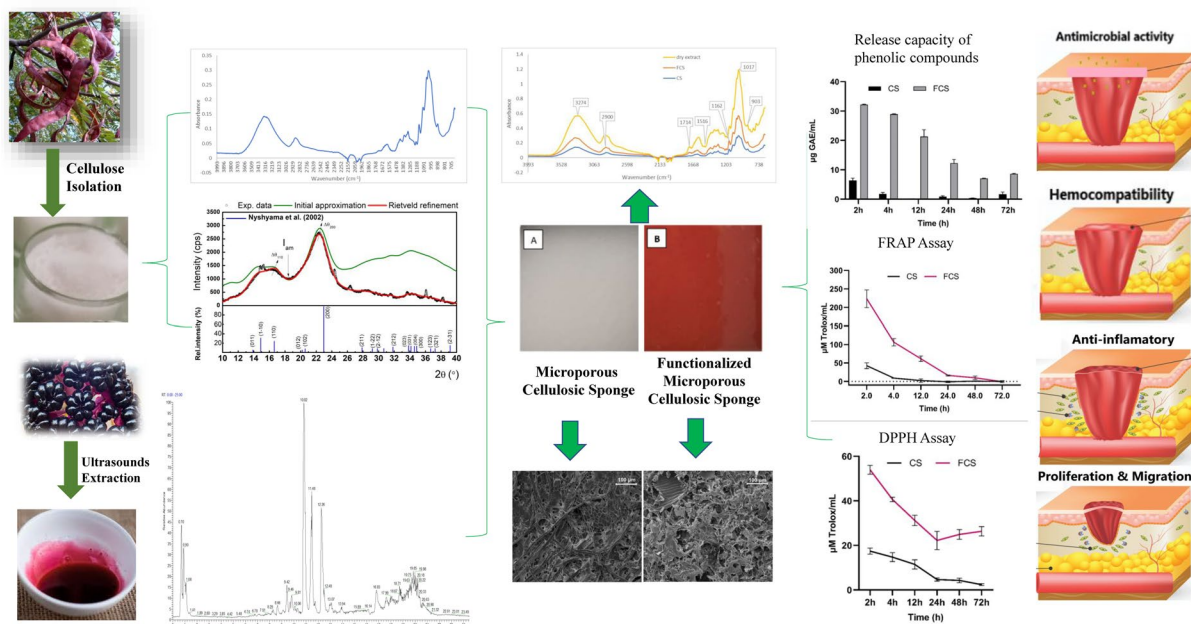
Keywords Microporous cellulosic sponge · Antioxidant activity · Antimicrobial activity · Biocompatibility · Hemocompatibility

Abbreviations

ATCC	American Type Culture Collection
ATR–FTIR	Attenuated total reflectance–Fourier transform infrared spectroscopy
CFU	Colony forming unit
CS	Microporous cellulosic sponge
COX-2	Cyclooxygenase-2
Cr.I	Degree of crystallinity
DI	Deionized water
DIBOA-glucoside	4-Hydroxy-3-oxo-3,4-dihydro-2H-1,4-benzoxazin-2-yl β-D-glucopyranoside
DMEM	Dulbecco's modified eagle medium
DPPH	2,2-Diphenyl-1-picrylhydrazyl
FRAP	Ferric reducing antioxidant power
GAE	Gallic acid equivalent
HESI	Heated electrospray ionization
IL	Interleukin
LDH	Lactate dehydrogenase
MRSA	Methicillin-Resistant *Staphylococcus aureus*
MTT	([3-(4,5-Dimethylthiazol-2yl)]-2,5-diphenyltetrazolium bromide)
FCS	Functionalized microporous cellulosic sponge
PBS	Phosphate-buffer solution
PWM	Pokeweed mitogen
RT	Retention time
SEM	Scanning electron microscopy
UHPLC–ESI–HRMS	Ultra-high-performance liquid chromatography–electrospray ionization–high resolution mass spectrometry

ROS	Reactive oxygen species
TPC	Total phenolic content
TPTZ	2,4,6-Tripyridin-2-yl-1,3,5-triazine
TE	Trolox equivalent
TIC	Total ion current
TNF	Tumor necrosis factor
vDIA	Variable data-independent analysis
XRD	X-ray diffraction

Introduction

Currently, wound management poses significant economic and clinical challenges, which explain the considerable interest in wound healing research and the development of more efficient therapeutic approaches. The wound healing could be impaired or delayed by the development of microbial biofilms, hyper or chronic inflammation, accumulation of free radicals (especially reactive oxygen species), and decreased mitogenic activity, inhibiting progression to proliferation and re-epithelialization (Shedoeva et al. 2019).

Along with technological progress, different wound dressings, such as hydrogels, hydrocolloids, alginates, tissue adhesives, porous adhesive films, and dressings containing silver and/or collagen, have been obtained (Dhivya et al. 2015). Many recent studies showed cellulose materials are appropriate for biomedical purposes due to their high biocompatibility (Dowsett and Newton 2005; Vartiainen et al. 2011; Alexandrescu et al. 2013; Rees et al. 2015). Being one of the most widespread compounds in nature, cellulose can be extracted from a wide range of sources (Moon et al. 2011; Fernandes et al. 2013), which mainly include plants and vegetal food waste, such as rice straw (Jianan et al. 1996), cannabis (Virtanen et al. 2012), cotton (Reddy and Yang 2009), wood (Cara et al. 2006), potato tubers (Abe and Yano 2009), banana peels (Phirom-on and Apiraksakorn 2022), pineapple (Fareez et al. 2018), etc. The performance characteristics of cellulose, such as its molecular chain length (degree of polymerization), size, degree of crystallinity, and thermal stability, depend on the plant source species, as well as the extraction method, including pre-treatment, post-treatment, and disintegration steps (Siqueira et al. 2010; Jeong et al. 2015; Lee et al. 2015; Trache et al. 2016). Although

bacterial and vegetal cellulose's chemical structure is similar, bacterial cellulose has a higher degree of crystallinity (> 80%) (Long et al. 2018).

Cellulose has a high chemical reactivity, allowing to obtain different derivatives, many of them multifunctional, using flexible preparation and numerous modification methods. The three main ways to modify cellulosic materials are: (i) adding active principles to the cellulose solution/suspension (Gawryla et al. 2009); (ii) depositing coatings on the cellulose gel surface using a sol–gel method; (iii) modifying the surfaces of cellulose aerogels by using a silane-type coupling agent and/or atomic layer deposition (Long et al. 2018).

Different cellulose materials have been reported, including nanofibrils bacterial cellulose, wood-derived cellulose (Martínez Ávila et al. 2014; Basu et al. 2018); nanofibers created by electrospinning, isolated from pineapple (Mahdavi et al. 2016; Souza et al. 2018); nanofibers (Di et al. 2017); nanocrystals derived from cotton (Catalán et al. 2015); nanorods derived from grass (Zhao et al. 2017); cellulose/nanosilver composite materials (Ye et al. 2016); cellulose/chitosan composite sponge (Liu et al. 2021); hierarchical porous cellulose sponge (Liu et al. 2022); carboxymethyl cellulose sponge (Paprskářová et al. 2021). Cellulose was intensively studied as a releasing active principles system for topical applications. The studies were generally carried out on commercial (carboxymethyl cellulose, hydroxyethylcellulose, ethylcellulose, cellulose acetate) or bacterial cellulose and not extracted from various plant matrices. Cellulose extracted from plant matrices has numerous applications for solving organic pollution (Han et al. 2016) and less often for topical applications. The functionalization was made with synthetic compounds with an antimicrobial effect (antibiotic), inorganic derivatives (Ag nanoparticles, silver sulfadiazine, ZnO nanoparticles) (Naseri-Nosar and Ziora 2018), and natural compounds such as curcumin (Bajpai et al. 2015, 2017), polyphenols from *Calendula officinalis* (Gustaite et al. 2015), polyphenols from *Camellia sinensis* (Shao et al. 2020), apple polyphenols (Lin et al. 2022) or larch bark polyphenols (Nie et al. 2022). The matrices functionalized with these compounds have in their composition two polymers that use cellulose in the form of microcrystals or CMC. Most of the cellulose-based materials with therapeutic applications were accomplished in

the form of strongly hydrophilic films, an essential characteristic for the exudate adsorption from wounds (Bajpai et al. 2015, 2017; Shao et al. 2020).

Invasive plants, which pose significant risks to biodiversity, the structure and functions of ecosystems, and the conservation of protected areas, could represent a cheap, readily available source of cellulose and active principles offering alternative and almost unlimited therapeutic options and, at the same time helping to limit their uncontrolled spread (Holloran 2006; Kumar Rai and Singh 2020). Among the invasive species, *Phytolacca americana* contains toxic compounds, especially in leaves and roots, that could cause pokeweed poisoning after oral administration. Symptoms include stomach burning, nausea, vomiting, and diarrhea (Ravikiran et al. 2011). However, the fruits are less toxic due to phytolaccatoxin and related triterpenes (Hamissou and Kurdmongkoltham 2015). As a result of their anti-inflammatory, antitumoral, and antimicrobial activity, *P. americana* extracts are used in folk medicine from Central and South America for treating inflammation, syphilis-associated pain, and other diseases (Gomes et al. 2008; Ravikiran et al. 2011). In addition, according to Patra et al. (2014), the crude extract of *P. americana* contains active substances that can inhibit the bacterial growth responsible for various oral diseases (Patra et al. 2014).

The mitogenic properties of *P. americana* extracts due to compounds such as the pokeweed mitogen lectin (PWM) isolated by saline extraction from pokeweed roots (Bodger et al. 1979; Bekeredjian-Ding et al. 2012) have been demonstrated since the 1960s by in vitro (Farnes et al. 1964) and in vivo assays (Barker et al. 1966).

However, for *P. americana* plant extracts, a release system is needed to avoid hemolysis which occurs at high concentrations. In this study, we address this limitation by using a cellulose matrix extracted from another invasive species, *G. triacanthos*, to encapsulate and release of the active principles contained in the *P. americana* fruit extract. This could lead to a cost-effective, circular bioeconomy and ecological approach to stop the uncontrolled spread of these two invasive species.

In this context, the present study characterizes cellulosic spongious materials from *G. triacanthos* pods that were functionalized with active principles from *P. americana* fruit extract. The potential of this

bioactive spongious material was established based on the in vitro determination of the wound healing accelerating effect, cytocompatibility, hemocompatibility, antimicrobial, antioxidant properties, and immunomodulatory activity.

Materials and methods

Materials

All chemicals ethanol (HPLC grade), formic acid (HPLC grade), methanol (HPLC grade), Folin–Ciocalteu's phenol reagent (2 M), sodium carbonate, gallic acid, cinnamic acid, chlorogenic acid, vanillic acid, syringic acid, ellagic acid, pinostrombin, que]rcetin, myricetin, 2,2-Diphenyl-1-picrylhydrazyl (DPPH), 2,4,6-tripyridyl-s-triazine (TPTZ), toluene (99.8% purity), sodium hypochlorite (6–14%), NaOH, lignin and Trolox (6-hydroxy-2,5,7,8-tetramethylchroman-2-carboxylic acid) were purchased from Sigma Aldrich (Germany). AgNO$_3$ (0.1 N) was purchased from Merck (Germany). All culture media (tryptone soy agar, Sabouraud agar, tryptone soy broth, Sabouraud broth and Muller–Hilton agar) were purchased from Oxoid (UK). All chemicals used were analytical grade.

Plant material

G. triacanthos pods and *P. americana* fruits (spontaneous flora) were harvested from Râmnicu Vâlcea and Bucharest, Romania, in September 2019. The voucher specimens are stored in Botanical Garden' Herbarium "Dimitrie Brândză" from the University of Bucharest (no. 40065 and no. 400712, respectively), where their taxonomic affiliation was certified too. The *G. triacanthos* pods were manually separated from other vegetative organs, slightly cleaned, and dried at 25 °C, while fresh *P. americana* fruits were used for extraction (on the same day after harvest).

Phenolic compounds from P. americana fruits—extraction and chemical composition

Phenolic compounds extraction from P. americana fruits

An amount of 5 g of previously milled fresh fruits was weighed, ethanol was used as a solvent, and the ultrasound-assisted extraction method was applied to obtain the extract. The final volume of the extract was brought to 50 mL with the same solvent. The sonication was repeated (for 30 min) and after that, the extract was maintained at 25 °C for 20 days, then filtered and stored at −20 °C until incorporation into cellulosic spongious material.

Total phenolic content (TPC)

The Folin–Ciocalteu method (Singleton and Rossi 1965) was applied to establish the TPC content, which was expressed as milligram gallic acid equivalent/mL extract (mg GAE/mL). Briefly, Folin–Ciocalteu reagent (0.1 mL) was mixed with extract, distilled water (1.8 mL), and saturated solution sodium carbonate (0.1 mL). After homogenization (15 s, at vortex), the solutions were kept in the dark for 60 min. Under the same conditions, the standard curve was drawn for different concentrations of gallic acid ($R^2 = 0.9985$). The absorbance was measured at 765 nm using a FlexStation 3 UV–VIS (Molecular devices Company, Sunnyvale, CA, USA) Spectrophotometer for samples or standard solutions.

Ultra-high-performance liquid chromatography– electrospray ionization–high resolution mass spectrometry (UHPLC–ESI–HRMS)

The quantitative analysis of phenolic compounds in the extract was performed using an UltiMate 3000 UHPLC system coupled to a Q-Exactive Focus Hybrid Quadrupole-OrbiTrap mass spectrometer equipped with heated electrospray ionization (HESI) probe (Thermo Scientific, Germany) set as described by Ciucure and Geană (2019). Separations was performed using a Kinetex (C18, 100×2.1 mm, 1.7 μm, Phenomenex, USA) column and a binary solvent system (A: water with 0.1% formic acid and B: methanol with 0.1% formic acid). Also, a screening UHPLC–MS/MS analysis was done to identify

specific compounds from *P. americana* fruit extract. Full scan data were acquired in negative mode covering a scan range of m/z 120–1800 at a resolving power of 70,000 FWHM at m/z 200, while variable data-independent analysis MS^2 (vDIA) was performed at the resolution of 35,000, isolation windows and scan set as follow: 120–305 m/z, 195–405 m/z, 295–505 m/z, 395–1000 m/z and 1000–1800 m/z. Data processing were performed with Compound Discoverer v. 2.1 Software, following an untargeted metabolomics working template.
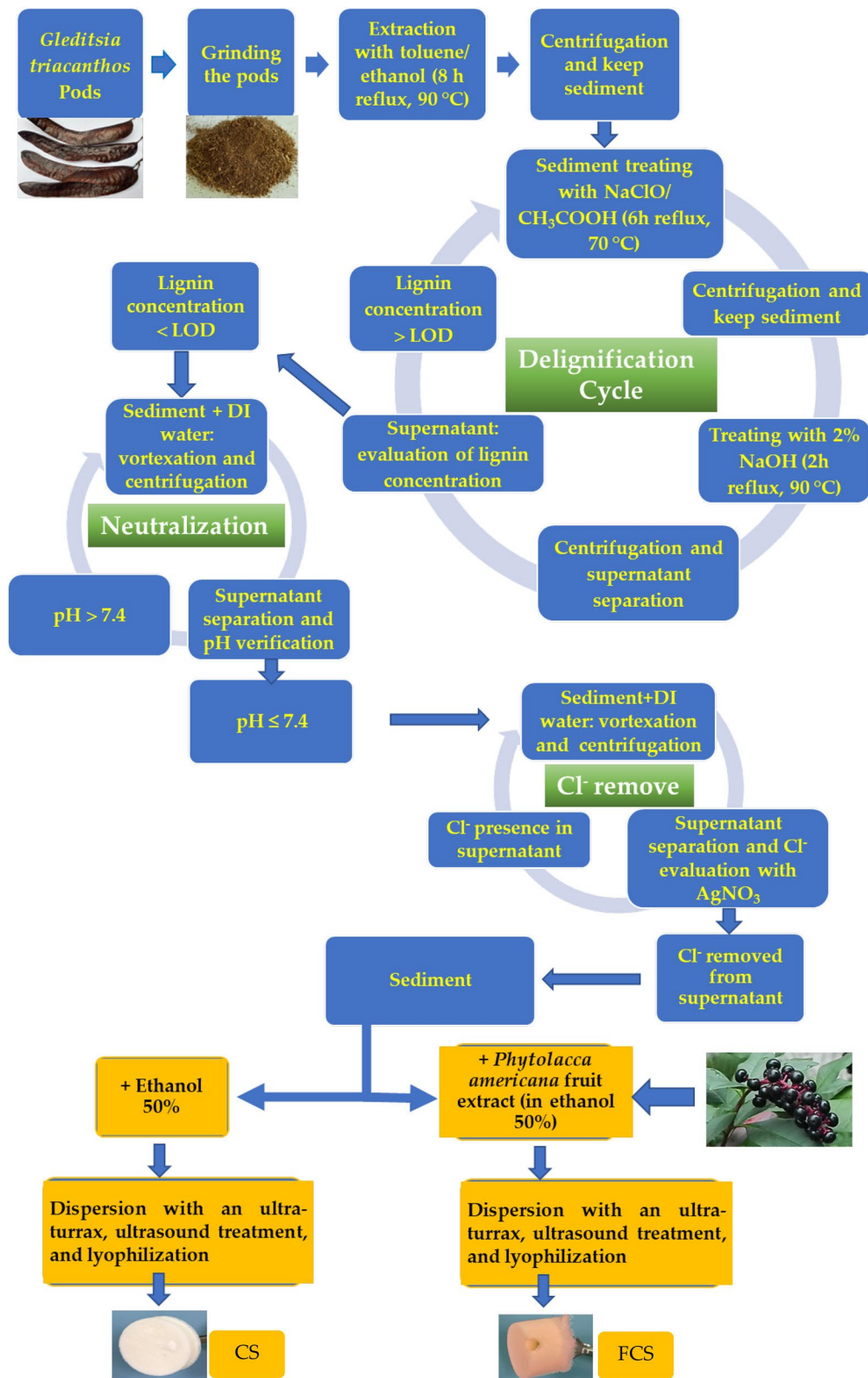
Microporous cellulosic sponge (CS) and functionalized microporous cellulosic sponge (FCS)—fabrication and characterization

The fabrication of CS and FCS

The cellulose extraction from 30 g *Gleditsia triacanthos* pods was carried out as presented by Zhuo et al. (2017), evaluating the presence of lignin after each cycle (n = 10). The extractable compounds were solubilized in toluene: ethanol (2:1, v:v) solution for 8 h at 90 ºC. A delignification cycle involved alternative reflux in the presence of sodium hypochlorite (70 ºC, heating on oil bath, 6 h) and NaOH 2% (90 ºC, 2 h). After each cycle, the biomass was centrifuged, washed with deionized water, and the total lignin content was quantified. The protocol used for total lignin (hydroxycinnamic acid method using lignin for calibration curve) content was done according to British Pharmacopoeia (Gaur et al. 2009). The supernatant was titrated with $AgNO_3$ to highlight the removal of chloride anions from the obtained cellulose solution. The washed cellulosic spongious material (approx. 2 g dry matter) was dispersed in the extract (4 mL) obtained previously, while for the control, ethanol (50%, 4 mL) was used. Then both were dispersed five times for ten minutes using IKA Ultra-Turax, followed by 30 min of sonication and freeze-drying to obtain the CS and the FCS, respectively. The schematic representation of the spongious materials fabrication stages is presented in Fig. 1.

Attenuated total reflectance–Fourier transform infrared (ATR–FTIR)

The Cary 630 FTIR Spectrometer in ATR mode and Agilent MicroLab Software FTIR System (Agilent

Gleditsia triacanthos Pods → Grinding the pods → Extraction with toluene/ethanol (8 h reflux, 90 °C) → Centrifugation and keep sediment → Sediment treating with NaClO/CH_3COOH (6h reflux, 70 °C)

Delignification Cycle

Centrifugation and keep sediment

Treating with 2% NaOH (2h reflux, 90 °C)

Centrifugation and supernatant separation

Supernatant: evaluation of lignin concentration

Lignin concentration > LOD

Lignin concentration < LOD

Neutralization

Sediment + DI water: vortexation and centrifugation

Supernatant separation and pH verification

pH > 7.4

pH ≤ 7.4 →

Cl⁻ remove

Sediment+DI water: vortexation and centrifugation

Cl⁻ presence in supernatant

Supernatant separation and Cl⁻ evaluation with $AgNO_3$

Cl⁻ removed from supernatant → Sediment

+ Ethanol 50%

+ *Phytolacca americana* fruit extract (in ethanol 50%)

Dispersion with an ultra-turrax, ultrasound treatment, and lyophilization → CS

Dispersion with an ultra-turrax, ultrasound treatment, and lyophilization → FCS

Technologies, Inc., USA) were used to record the FTIR spectra for CS, FCS, and dry extract. 4000–650 cm^{-1} was the selected measurement range, with 400 scans and a resolution of 4 cm^{-1}.

X-ray diffraction

The X-ray diffraction (XRD) pattern was recorded using a laboratory Rigaku SmartLab (Osaka, Japan) X-ray diffractometer with nominal power of 9 kW, which provides monochromatic X-rays with wavelength, $\lambda = 0.15418$ nm. The XRD measurement was performed in grazing incidence configuration, for which the incidence angle of the source was kept at 0.5°, while the detector moved from 5 to 70°. During the acquisition, a speed of 2.5°/min was used, while the scan step was 0.05°.

Morphology of CS and FCS

The morphological features of CS and FCS were acquired using a Nova NanoSEM 630 Scanning Electron Microscope (FEI Company, Hillsboro, OR, USA) using an accelerating voltage of 10 kx. For the SEM images, all samples were coat-sputtered with Au to ensure the conductivity of the sample.

Surface wettability

Static (equilibrium) CAs were carried out at 25 °C, and a drop shape analysis instrument, model DSA100 (Krüss GmbH, Hamburg, Germany), was used. The analysis was performed according to Stan et al. (2020).

Water absorption and retention properties

The method was adapted after Ngadaonye et al. (2013). Briefly, 0.1 g CS or FCS was submerged in phosphate buffer solution (PBS) (pH 7.4, 37 °C, for 15 min). The PBS excess was taken away with filter paper, and the material's wet mass was determined. Then, the swelling ratio (%) for CS and FCS was calculated according to Ngadaonye et al. (2013).

For fluid retention tests, the samples (CS and FCS) were taken in PBS for 24 h at 37 °C, and the excess solution was removed with filter paper. The samples were maintained at 37 °C and weighed at different time points (1, 2, 3, 4, 5, 6, 12, 24, and 48 h) (Lu et al. 2016). Finally, the equation applied was done according to Marinas et al. (2020).

In vitro *release studies for phenolic compounds and their antioxidant activity*

The FCS were immersed in PBS for five days at 37 °C in dark glass vessels containing 1 mL PBS to analyze phenolic compounds' release kinetics. The release studies were conducted by replacing the medium with fresh PBS at each sampling time point (at 2, 4, 6, 24, 48, and 72 h). The release of the active principles was quantified by Folin–Ciocalteu, 2,2-Diphenyl-1-picrylhydrazyl (DPPH), and Ferric Reducing Antioxidant Power (FRAP) methods with a FlexStation 3 UV–VIS Spectrophotometer (molecular devices company, Sunnyvale, CA, USA). Total phenolic content was determined according to 2.2.2.

DPPH assay

A previously reported method with slight changes was applied (Madhu et al. 2013). The reaction mixture consisted of 100 μL of sample and 100 μL DPPH solution, incubated for 30 min in the dark. The absorbance was measured at 517 nm. A Trolox solution (0–200 μM concentrations) was used for the standard curve ($R^2 = 0.9982$). The antioxidant activity was expressed as mM TE (Trolox Equivalent)/g material.

FRAP assay

The FRAP method was performed according to Benzie and Strain (1996) with some modifications (Thaipong et al. 2006). The FRAP reagent was prepared as follows: 300 mM acetate buffer (pH 3.6), 10 mM 2,4,6-tripyridin-2-yl-1,3,5-triazine (TPTZ) stock solution in 40 mM HCl and 20 mM FeCl$_3$ solution in water were mixed in 10:1:1 (v:v:v) ratio. The FRAP reagent was freshly prepared and kept at 37 °C. Over 15 μL sample or standard solution, 285 μL FRAP reagent was added and incubated for 30 min at 37 °C in the dark. The absorbance at $\lambda = 593$ nm was read. The standard curve was linear

between 0 and 250 μM Trolox ($R^2=0.9968$). Results were expressed as millimolar TE/g material.

Antimicrobial activity

Sterilization of CS and FCS

The CS and FCS were sterilized by irradiation, the doses absorbed by the samples ranging between D min$=33.2\pm1.6$ kGy and D max$=35.7\pm1.6$ kGy. The used dosimetry system consisted in ethanol chlorobenzene (ECB) mixture. Gamma irradiation (Co-60) was performed for around 12 h at a dose greater than 25 kGy using SVST Co-60/B irradiator (Institute of Isotopes Co. Ltd. Budapest, Hungary). The sterility verification was done at 10% CS in peptone water and maintained at 37 °C for 24 h, and 100 μL was inoculated on tryptone soy agar and Sabouraud agar. Finally, the Petri plates were incubated at 30 °C for 72 h for the enumeration of aerobic and mesophilic microorganisms and seven days for fungi.

Evaluation of the antimicrobial activity

The following strains were used: *Escherichia coli* ATCC 11229*; Staphylococcus aureus* ATCC 6538*; Enterococcus faecium* DMS 13590*, Pseudomonas aeruginosa* ATCC 27853*; Candida parapsilosis* ATCC 22019 and *Candida albicans* ATCC 10231 as well as clinical, multi-drug resistant isolates, *i.e., Staphylococcus aureus, Pseudomonas aeruginosa, Acinetobacter baumannii* and *Enterobacter cloacae*, from the microbial collection of Microbiology Laboratory from Faculty of Biology, University of Bucharest (Ong et al. 2008). The CS and FCS samples were submerged with microbial suspension (10^4 CFU/mL) and vortexed. The viable cell counts (CFU/mL) were determined on solid media (Muller–Hinton agar for bacteria and Sabouraud for yeasts) at initial (around 10 min) and one-day contact times. The method was adapted from SR EN ISO 11737-1 (2006) Sterilization of medical devices—Microbiological methods—Part 1: Determination of a population of microorganisms on products. The logarithmic reduction of microbial growth was calculated as follows:

$$\text{Recovery rate} = \frac{lg(CFU_{sample})}{lg(CFU_{controlstrain})} \quad (1)$$

Assessment of the anti-inflammatory effect and biocompatibility

Cytotoxicity and cell proliferation

Hep-2 (Human Epithelial Cell Line, ATCC) and RAW 264.7 (macrophage-like, Abelson leukemia virus-transformed cell line derived from BALB/c mice, ATCC) cells were cultured in Gibco Dulbecco's Modified Eagle Medium (DMEM) supplemented with 10% fetal bovine serum and Penicillin–Streptomycin (100 U/mL) and Amphotericin B (25 μg/mL). CS and FCS were weighted in sterile saline buffer. The tested concentrations were 25, 50, 150, 250 and 500 μg material/mL. Cytotoxicity was assessed using the Cytotoxicity Detection Kit (Sigma–Aldrich) based on the measurement of the LDH released from damaged cells. Cell proliferation was analyzed with the Cell Proliferation Kit I (MTT, Sigma–Aldrich) (Serbezeanu et al. 2019).

Pro-wound healing activity

Using a previously described method, the standard Hep-2 cell line, recommended for routine testing of biomaterials cytocompatibility, was used to test the new materials effect on wound healing (Muniandy et al. 2018). The Hep-2 cell line is also recommended for the scratch assay (Takumi-Tanimukai et al. 2022) because these cells easily form a confluent monolayer. The CS and FCS were tested at 100 μg/mL concentration, for which they show the highest level of biocompatibility. Image analysis was performed using the Image J software.

Immunomodulatory activity

The RAW 264.7 cells (10^5 cells/well) were stimulated with *E. coli* (10^6 CFUs/well) or with *E. coli* supplemented with CS/FCS (100 μg/mL). After 2 h of stimulation, supernatants were taken and analyzed for IL-6 and IL-10 production using ELISA kits (Invitrogen).

Hemocompatibility

The hemolysis test was made according to Jiang et al. (2011) with few modifications. A 4 mL volume of whole bovine blood treated with 10% citric

acid dextrose (CDA) was diluted with 5 mL of 0.9% PBS. An amount of 10 mg CS and FCS respectively, was incubated in PBS for 30 min at 37 °C. After adding diluted blood (0.05 mL) to each sample the tubes were incubated for 60 min at 37 °C. Positive and negative controls were performed by adding 0.05 mL of bovine blood to 0.5 mL of distilled water (negative control) and PBS (positive control), respectively. All tubes were centrifuged for 5 min. The absorbance (A) of the supernatant was measured at 545 nm. Hemolysis was calculated as follows (Reshmi et al. 2018):

$$\text{Hemolysis} = \frac{A_{\text{sample}} - A_{\text{control}(-)}}{A_{\text{control}(+)} - A_{\text{control}(-)}} \times 100 \qquad (2)$$

For the blood clotting tests, a 5 µL volume of bovine blood was spotted over 10 mg of material. The blood was allowed to coagulate on the substrates for 60 min, and the free hemoglobin concentration was measured at 10 min. To measure the concentration of free hemoglobin lysis, the substrates were immersed in 500 µL of deionized water (DI). The substrates were gently shaken and left in DI water for 5 min to lyse free hemoglobin. The absorbance was measured at a wavelength of 540 nm. The absorbance value increases with the concentration of free hemoglobin (Smith et al. 2010).

Statistical analysis

Data were expressed as means $\pm$ SD determined by triplicate analysis. The GraphPad Prism v9 software was used for statistical analysis. Ordinary two-way ANOVA with two-stage linear step-up procedure with individual variances method was assessed for comparison between CS and FCS (for water retention, phenols release, antioxidant activity, antimicrobial activity, hemolysis, blood clotting, wound closure, LDH release, cell proliferation, and cell migration). For immunomodulatory activity, the results were analyzed using ordinary two-way ANOVA with main effects by Tukey's multiple comparisons assay for each comparison between native cells stimulated with *E. coli* and CS or FCS. The significant level was set to *p*-values < 0.05.

Results and discussion

Chemical characterization of P. americana fruit extract

The quantification of TPC was done using the calibration curve for gallic acid, obtaining a content of 477.86 ± 6.19 µg TPC (GAE, gallic acid equivalents)/mL extract.

The main phenolic acids quantified in the alcoholic extract of *P. americana* fruits were cinnamic acid (1019.98 µg/L), chlorogenic acid (283.65 µg/L), vanillic acid (104.28 µg/L), syringic acid (99.31 µg/L) and ellagic acid (73.99 µg/L), while pinostrombin (156.80 µg/L), quercetin (64.36 µg/L) and myricetin (43.26 µg/L) were the most abundant flavonoids. The concentrations of phenolic acids, flavonoids, and flavonoid heterosides are shown in Table S1.

The screening UHPLC–Q–Orbitrap HRMS analysis allowed to identify many bioactive compounds and their metabolites present in the *P. americana* extract, which are also responsible for antioxidant activity. In addition, data processing using Compound Discoverer Software allowed the identification of the compounds found in the extract by searching in online libraries and databases, such as Chemspider, mzCloud, MzVault and mass list matches (Hohrenk et al. 2020).

Chemical compounds such as phenolic acids, flavonoids, isoflavones, anthocyanidin derivatives and gibberellin plant hormones, but also organic acids and vitamins, could be identified in *P. americana* fruit extract. Table 1 shows the molecular formula and the retention time of the main identified compounds based on the mass-to-charge ratio (m/z) and MS/MS fragment formed during ESI in negative mode. Most identified compounds showed antimicrobial and anti-inflammatory properties (Bailly 2021), and anti-allergic effects (Chen et al. 2022), suggesting their efficacy in the treating skin health problems.

Attempts were made to identify the saponins in the extract obtained from *P. americana* fruits based on a UHPLC–ESI–HRMS analysis. The total ion current (TIC) chromatogram of the *P. americana* fruit extract in the negative ion mode, covering a scan range between 120 and 1800 m/z, is shown in Fig. S1. The extracted chromatograms of the main saponin compounds identified in the *P. americana* extract using a 5 ppm mass accuracy window are presented in Fig.

Table 1 The chemical compounds identification in *P. americana* fruit extract based on UHPLC–ESI–HRMS analysis combined with data processing using compound discoverer software

Compound name	Formula	R.T. (min)	Exact mass	Accurate mass [M-H]$^-$	Experimental adduct ion (m/z)	MS^2 fragments (m/z)
Azelaic acid	$C_9H_{16}O_4$	9.82	188.10486	187.0976	187.0969	165.0546, 135.0348, 147.0349, 068.0737
Suberic acid	$C_8H_{14}O_4$	9.00	174.08921	173.0820	173.0812	137.0231, 130.0860, 92.9266
Quercetin-3-O-glucoside (isoquercetin)	$C_{21}H_{20}O_{12}$	9.44	464.09548	463.0882	463.0881	300.0273, 165.0546, 289.9205, 135.0439
Delphinidin-3-O-glucoside	$C_{21}H_{20}O_{12}$	9.47	464.09548	463.0882	463.0881	165.0547, 147.0440, 135.0439
Cyanidin-5-O-glucoside	$C_{21}H_{20}O_{11}$	9.84	448.10056	447.0933	447.0934	329.1031, 284.0325, 163.0392
3′,5-Dihydroxy-3,4′,7-trimethoxyflavone	$C_{18}H_{16}O_7$	9.79	344.0896	343.0823	343.0825	165.0546, 147.0440, 135.0439
7-Hydroxy-2′,4′,5′-trimethoxyisoflavone	$C_{18}H_{16}O_6$	10.18	328.09469	327.0874	327.0877	165.0390, 162.0311, 147.0440, 165.0546
Taxiphyllin	$C_{14}H_{17}NO_7$	8.36	311.1005	310.0932	310.0931	121.0282, 147.0440, 159.0441, 269.0819
Afrormosin	$C_{17}H_{14}O_5$	8.71	298.08412	297.0769	297.0767	137.0231
Saponarin	$C_{27}H_{30}O_{15}$	9.28	594.1584	593.1511	593.1517	284.0328, 297.0770, 304.9143
Gibberellin A36	$C_{20}H_{26}O_6$	13.32	362.17294	361.1657	361.1666	137.0232
Gibberellin A19	$C_{20}H_{26}O_6$	18.51	362.17294	361.1657	361.167	325.1842, 183.0112, 96.9586
(−)-Usnic acid	$C_{18}H_{16}O_7$	9.05	344.0896	343.0823	343.0821	163.0390, 137.0232, 92.9266
DIBOA-glucoside	$C_{14}H_{17}NO_9$	7.09	343.09033	342.0831	342.0833	180.0292, 152.0341
9-Demethylmunduserone	$C_{18}H_{16}O_6$	9.87	328.09469	327.0874	327.0876	165.0546, 147.0440, 135.0439
Pregna-4,9(11)-diene-3,20-di-one	$C_{21}H_{28}O_2$	17.46	312.20893	311.2017	311.2018	96.9587, 149.0960, 183.0112, 265.1478
[6]-Gingerol	$C_{17}H_{26}O_4$	18.51	294.18311	293.1759	293.1794	183.0112, 96.9586
(−)-Medicarpin	$C_{16}H_{14}O_4$	8.24	270.08921	269.0820	269.0823	121.0281, 162.8380, 160.8409, 159.0440
Citric acid	$C_6H_8O_7$	0.94	192.027	191.0197	191.0186	191.0186, 111.0073, 87.0073
(−)Threo-iso(homo)2citrate	$C_8H_{12}O_7$	5.83	220.0583	219.0510	219.0504	162.8380, 160.8409, 111.0074, 72.9916
Dihomocitrate	$C_8H_{12}O_7$	6.72	220.0583	219.0510	219.0507	11.0074, 162.8380, 160.8409, 87.0073
Pantothenic acid (vitamin B$_5$)	$C_9H_{17}NO_5$	5.75	219.11067	218.1034	218.1028	152.0341, 146.9599, 144.8685, 92.9266

R.T.–retention time

S2. The retention times, precursor ion mass, and fragment ion data of these compounds are summarized in Table 2.

Thus, nine esculentosides (A, B, H, M, S, R, L, G, and F) were identified in *P. americana* fruit extract, from which A, B, and H, were the most abundant. Esculentoside compounds show strong anti-inflammatory (Wei et al. 2015; Saleri et al. 2017), anti-allergic (Ci et al. 2015), anti-cancer (Saleri et al. 2017; Bailly and Vergoten 2020), antifungal and antiviral, including against SARS-COV-2 (Zeng et al. 2021) effects. In addition, the antifungal saponins phytolaccoside F and phytolaccasaponin N-5, but also phytolaccagenin, widely used to treat inflammatory conditions (Wei et al. 2015), as well as triterpene glycosides (desholothurin and holothurinoside) which have considerable antitumor and antiviral activities (Bordbar et al. 2011) were also identified in the *P. americana* fruit extract. Phytolaccagenin, desholothurin and holothurinoside, are biologically-active

Cellulose (2023) 30:10313–10339
10323

Table 2 Identification of triterpenoid saponins in *P. americana* fruits based on UHPLC–ESI–HRMS analysis combined with data processing using Compound Discoverer Software

Compound name	Formula	R.T. (min)	Exact mass	Accurate mass [M-H]$^-$	Experimental adduct ion (m/z)	MS^2 fragments (m/z)
Esculentoside A	$C_{42}H_{66}O_{16}$	10.80	826.4350	825.4277	825. 4280	825.4283, 663.3755, 531.3327
Esculentoside B	$C_{36}H_{56}O_{11}$	13.63	664.3822	663.3749	663.3759	304.9142, 242.9433, 232.9145
Esculentoside H	$C_{48}H_{76}O_{21}$	10.82	988.4879	987.4806	987.4802	824.4279, 663.3751, 531.3326
Esculentoside M	$C_{48}H_{74}O_{22}$	11.15	1002.4671	1001.4593	1001.4603	825. 4293
Esculentoside S	$C_{42}H_{66}O_{15}$	12.97	810.4401	663.3744	809.4323	809.4332, 647.3807, 515.3379
Esculentoside R	$C_{54}H_{86}O_{24}$	12.26	1118.5509	1163.5480	1163.5480	1153.5200, 955.4910
Esculentoside L	$C_{48}H_{76}O_{20}$	12.97	972.4929	971.4856	971.4865	809.4336, 647.3808, 515.3379
Esculentoside G	$C_{48}H_{74}O_{21}$	10.29	986.4722	985.4644	985.4659	832.4130, 643.3490, 529.3173, 329.1033
Phytolaccoside F	$C_{48}H_{76}O_{19}$	13.07	956.4981	955.4908	955.4903	809.4338, 647.3807, 515.3376
Phytolaccasaponin N-5	$C_{54}H_{86}O_{25}$	11.33	1134.5457	1133.5384	1133.5387	971.4862,
Phytolaccagenin	$C_{31}H_{48}O_7$	14.37	532.3400	531.3327	531.3331	531.3331
Desholothurin	$C_{54}H_{86}O_{24}$	13.07	1118.5509	1117.5436	1117.5441	955.4918, 809.4338, 1153.5212
Holothurinoside	$C_{60}H_{96}O_{29}$	10.98	1280.6037	1279.5964	1279.5968	1279.5968, 1023.4577, 987.4810, 825.4286

R.T.–retention time
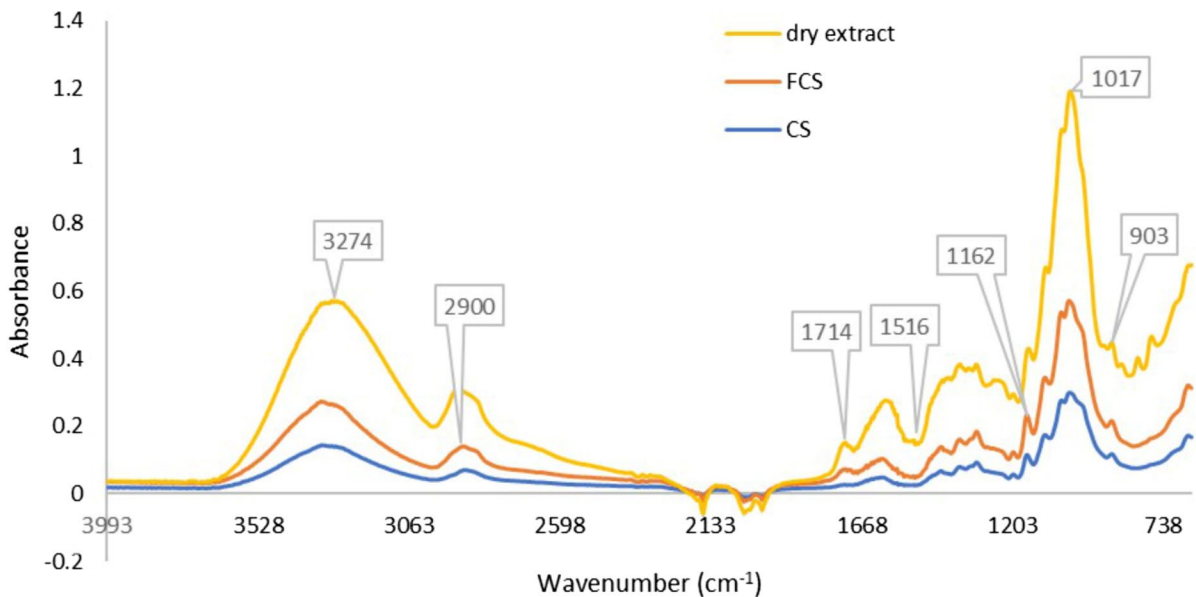
Fig. 2 FTIR spectra of microporous cellulosic sponge (CS) and functionalized microporous cellulosic sponge (FCS)

surfactants in plants, acting as bacterial growth inhibitors (Chen et al. 2022).

Characterization of microporous cellulosic sponge (CS) and functionalized microporous cellulosic sponge (FCS)

Fig. 3 Experimental XRD pattern (black line) and the Rietveld fit (red line) with the fitting parameters. Theoretical positions of (hkl) reflections of Nishiyama cellulose are displayed to confirm the cellulose I_β diffraction peaks. The input model (olive line) was proposed based on Nishiyama cellulose (66.7%) and amorphous part (33.3%)
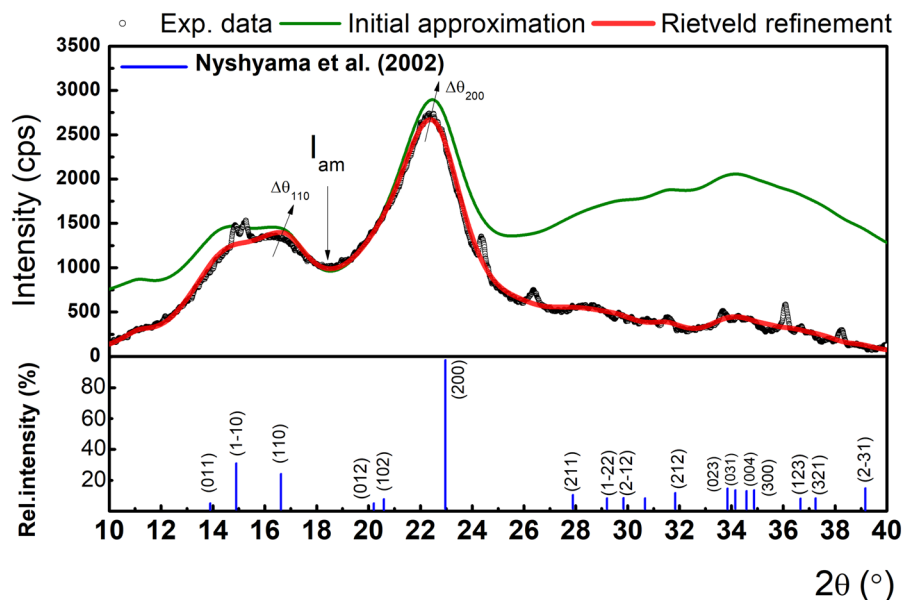
Pods from different vegetables have high cellulose, hemicellulose, and lignin content. In our previous studies, we extracted cellulose (Marinas et al. 2020) and obtained microfibers. In this study, the pods' powder was submitted to ten cycles of delignification to remove the extractable substances, hemicellulose, and lignin. After extraction, the lyophilized cellulosic spongious material ($15.33 \pm 2.52\%$ from total pods powder) was characterized and compared with the nanocellulose functionalized with phenolic compounds extracted from *P. americana* fruits (Fig. 1).

The ATR–FTIR spectra of the studied materials, CS and FCS, are presented in Fig. 2. According to Garside and Wyeth (2003), the absence of the C=O band observed in both spectra (at ~ 1735 cm^{-1}) shows the complete hemicellulose removal. The lack of bands at ~ 1505 cm^{-1} and ~ 1595 cm^{-1} (aromatic C=C vibrations in the plane) and 1263 cm^{-1} (C–O–C specific to etheric bonds) highlights the successful removal of lignin. The glycosidic ether bands C–O–C (~ 1160 cm^{-1}) are specific for the presence of cellulose. The band from ~ 2900 cm^{-1}, detected in all samples, corresponds to the C–H stretching vibration from the organic content (Garside and Wyeth 2003). The OH group specific to primary alcohols comes from the ethanol solvent, tested at a similar concentration to that used to obtain the *P. americana* fruit extract.

According to the literature data (Edelmann et al. 2001; Fernández and Agosin 2007), the bands in the region 1680–900 cm^{-1} are specific to phenolic compounds from the extract. The specific aromatic C–H vibrations are attributed to the wavenumbers between 670–900 cm^{-1} and 950–1225 cm^{-1} (Laghi et al. 2011). Also, the wavenumber 902 cm^{-1} can be attributed to the saponoside components in the composition of *P. americana* fruit extract (Hajimohammadi et al. 2016). The presence of fruits-specific beta-cyanides can be identified at the wave numbers 3274 cm^{-1} (range O–H and N–H), 1712 cm^{-1} (range C=O), and 1516 cm^{-1} (range C=C) (Qin et al. 2020). Table S2 gives the main absorption bands and their assignments for CS, FCS and dry extract.

Further, structural features of the investigated sample were assessed using X-ray diffraction. In Fig. 3 is presented the experimental XRD pattern (black line), which exhibits a main diffraction peak located at 22.3°, accompanied by broad diffraction features at ~ 15°, 16.5°, 28.4° and 34.2°. Besides, diffraction peaks with small intensity can be observed.

The broad features were assigned as different (hkl) reflections of cellulose I_β, according to the.cif file (Nishiyama et al. 2002; French 2014) (see blue lines that corresponds to the main reflections of I_β), with 2θ = 13.80°, 14.28°, 14.82°, 16.66°, 18.69°, 20.25°,

20.59°, 22.97°, 27.98°, 29.14°, 29.84°, 30.63°, 31.80°, 33.84°, 34.13°, 34.54°, 34.87°, 36.62°, 37.24° and 38.18°). In addition, unidentified sharp diffraction peaks could be given by the presence of phenolic compounds, specific to the fruit extract. For instance, Rathi et al. (2019) showed that the cinnamic acid presents a couple of diffraction peaks in the range of 10–35°, this being the main phenolic acid quantified in the alcoholic extract of *P. americana* fruits.

A key structural parameter for cellulose is the crystallinity degree (index), which is closely related to the rigidity/flexibility of cellulose fibers. For instance, Gümüşkaya et al. (2003) showed that the rigidity and flexibility are closely related by the crystallinity degree given by hemicelluloses and lignin (Carrión-Prieto et al. 2019). The degree of crystallinity (Cr.I) was evaluated using the empirical equation proposed by Segal et al. (1959) through the following equation:

$$Cr.I = \frac{I_{200} - I_{am}}{I_{200}} \times 100 \qquad (3)$$

where I_{200} represents the peak intensity corresponding to the crystalline domain and I_{am} to the minimum intensity between (110) and (200) located at 18.4°. Accordingly, a degree of crystallinity of 66.7% has been obtained.

Another central structural aspect is related to the size of the crystalline domains, since the different crystallite sizes affect the thermal degradation temperature of natural fibers (Poletto et al. 2013). One of the most common ways to evaluate the crystal quality is based on the Scherrer's equation on the (200) main reflection that gives the correlation between the size of the crystalline domains and the Full Width at Half Maximum (FWHM) (Patterson 1939):

$$\tau = \frac{k\lambda}{\beta \cos \theta} \qquad (4)$$

where k is a shape factor usually taken as 0.93, λ is the wavelength of the incident X-ray beam (0.15418 nm), β is the Full Width at Half Maximum (FWHM) of the diffraction peak in radians and θ is the angular position. Based on the pseudo-Voigt fit of the (200) cellulose reflection, the FWHM is 2.8°, which implies a mean crystallite size of 3.3 nm. Further insights related to the mean crystallite size and the lattice strain were gained using the Whole Powder Pattern Fitting (Rietveld) method using PDXL: Integrated

X-ray powder diffraction software developed by Rigaku corporation (https://www.rigaku.com/techniques/rietveld-analysis). After publication of the crystal structure of I_β by Nishiyama et al. (2002), the Rietveld method was applied by a number of researchers (Thygesen et al. 2005; Driemeier and Calligaris 2011; Driemeier 2014; Duchemin 2017). Here, the pattern fitting is performed over a broad angular range, based on information about the crystal system and lattice constants (Rietveld 1967, 1969). Thus, it requires to have a reasonable initial approximation of some parameters, including peak shape, unit cell dimensions, or coordinates of all atoms in the crystal structure, to resolve a real structure (Pecharsky and Zavalij 2008; French 2020). In Fig. 3, an initial model (olive line) was proposed in the assumption of two well-defined phases: (1) crystalline Nishiyama cellulose I_β with theoretical positions displayed with blue lines and (2) amorphous state with crystallinity index of 67.7%, contributing to background. In this framework, the Rietveld method includes the smaller peaks that are lost in what appears to be background or amorphous scattering (French 2020). Extensive reports were published related to the shape of the amorphous scattering in cellulose. So far, in the literature is no standard model for amorphous cellulose and common peak functions such as Gauss, Lorentz and Voigt functions do not fit the amorphous profile well. It was shown that the amorphous contribution to the diffraction pattern is more complex than a simple shape. For instance, (Thygesen et al. 2005) used a 10-parameter Chebychev polynomial function that included background. A new peak deconvolution method was proposed to analyze cellulose XRD data with the amorphous Fourier model function in conjunction with standard Voigt functions representing the crystalline peaks (Yao et al. 2020). Concomitantly, del Cerro et al. used nine Gaussian functions to represent the amorphous fraction (del Cerro et al. 2020). In this work, the Rietveld refinement using PDXL: Integrated X-ray powder diffraction commercial software was used to refine the amorphous XRD scattering, as well as the entire XRD pattern. In fact, it implies fitting of the experimental data with a theoretical profile, y_i^{calc} with the following expression (Pecharsky and Zavalij 2008):

$$y_i^{calc} = A(2\theta) \sum_n s_n \sum_{\boldsymbol{h}} P_{n,\boldsymbol{h}} I_{n,\boldsymbol{h}} \phi_n(2\theta_i - 2\theta_h - T(2\theta_i)) + y_b(2\theta_i)$$

(5)

Here, s_n is the scale factor, $2\theta_h$ the Bragg angle, $A(2\theta)$ the absorption and irradiation correction, $P_{n,\boldsymbol{h}}$ the preferred orientation correction, $I_{n,\boldsymbol{h}}$ the integrated intensity function, $T(2\theta_i)$ the angular correction, and $y_b(2\theta_i)$ the background function. During the refinement, the background was modelled with a B-spline function, the peak shift with the shift axial displacement model, the peak shapes using pseudo-Voigt fits, while the preferred orientation with the March–Dollase function. One can notice that the initial approximation fits adequately the amorphous

intensity of the experimental data (I_{am}), as well as the (110) and (200) reflections. This fact clearly indicates that the calculated crystallization index by Eq. (3) was successfully incorporated in the initial approximation. On the other hand, the initial approximation fails in the description of the secondary reflections located at higher 2θ angles. In addition, the Rietveld refinement considers the actual main crystalline parameters, such as the unit cell parameters, mean crystallite size, lattice strain or preferential orientation. The observed discrepancies
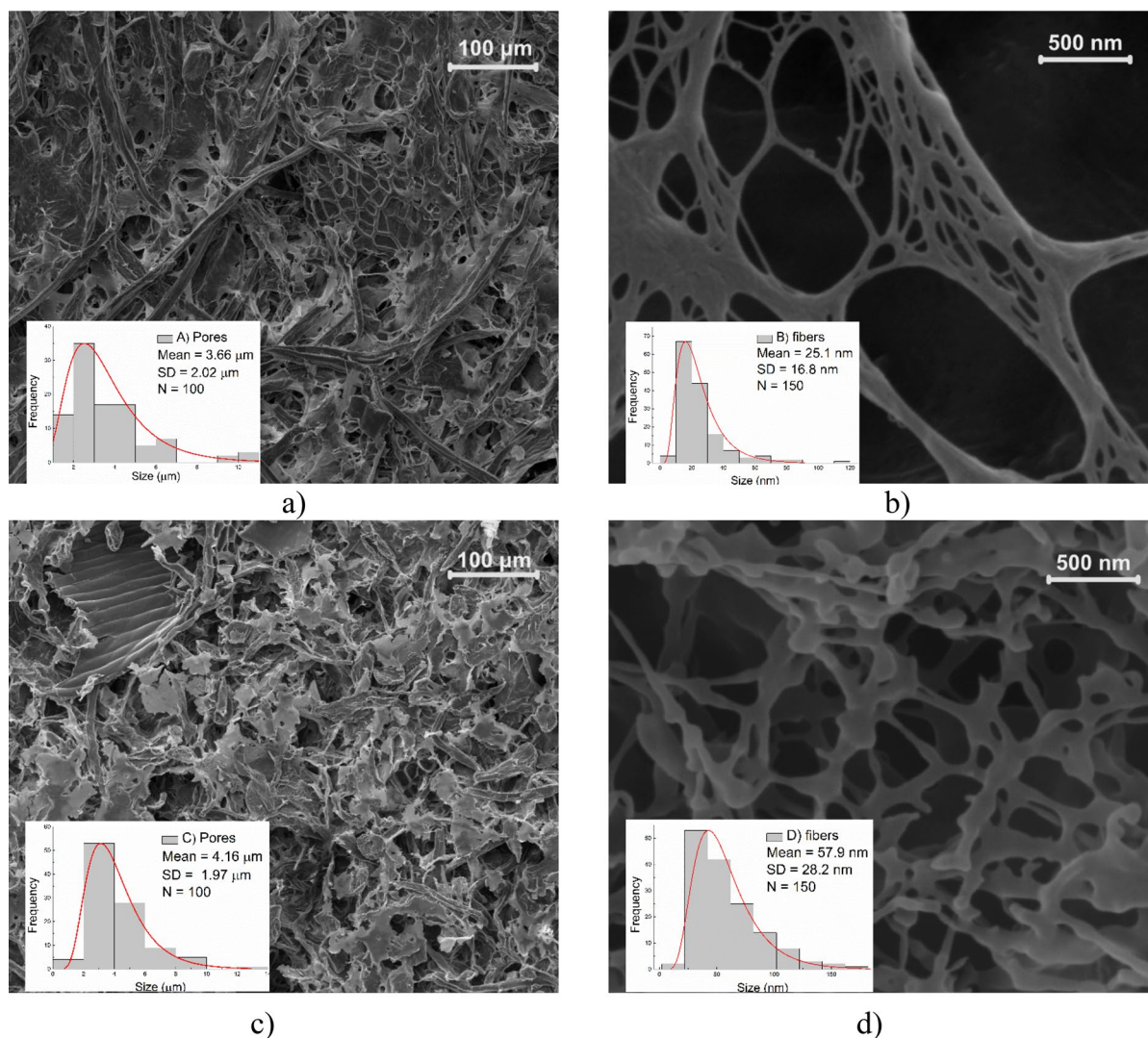
Fig. 4 The SEM images of the reference CS surface (**a** 100 K×magnification, inset A—pore size histogram; **b** 500×magnification, inset B—fibers size histogram) and the FCS surface (**c** 100 K×magnification, inset C—pore size histogram; **d** 500×magnification, inset D—fibers size histogram)

between the initial approximation and experimental data result from either preferential orientation along (200) or due to a non-negligible strain in the cellulose lattice, reflected in the relative intensities of the reflections related to the (200) and shift of the diffraction peaks, respectively. The shift between the initial approximation and the experimental data, Δθ is evidenced using black arrows, indicating that the actual interplanar distance of (110) and (200) atomic planes is slightly expanded, probably due to a non-negligible tensile lattice strain. By means of the Rietveld refinement, the diffraction feature positions are well-described, as well as the relative intensities of the secondary diffraction peaks (i.e,. others than (200)). During the least squares fit, four numerical figures of merit (FOM's) were used: reliability factor (R_p), the weighted parameter (R_{wp}), the expected profile residual, Re and the goodness of the fit, χ^2, showing the reliability of the fit. For the present fit, the following FOM's were obtained: $R_p = 3.60\%$, $R_{wp} = 4.83\%$, $R_e = 2.98\%$ and $\chi^2 = 2.62$.

The discrepancies between Rietveld and experimental data reside in: (1) the presence of the crystalline phase, ascribed to the cinnamic acid, as well as (2) unresolved overlapped diffraction peaks due to the presence of the amorphous phase. In fact, Rietveld analysis proves the existence of the type I_β cellulose with monoclinic symmetry in the investigated sample, with lattice unit parameters a = 7.784 Å, b = 8.201 Å, c = 10.38 Å nm with γ = 90°. Based on the Rietveld fit, a mean crystallite size of 2.6 nm was obtained, and at the same time, a tensile lattice strain of 1.6%. At the same time, the Scherrer equation gave a mean crystallite size of 3.3 nm, both values being typically for cellulose (Thygesen et al. 2005).

Figure 4 shows the morphologies of microporous cellulosic sponge (CS—a and b) and functionalized microporous cellulosic sponge (FCS—c and d). In the insets are illustrated the histograms of the pore diameter (Fig. 4A and C) and the nanofibers' diameter (Fig. 4B and D). The SEM images show two areas in both samples: microporous material and a smaller area that presents cellulose nanofibers. The size distribution of the CS (Fig. 4a, b) and FCS (Fig. 4c, d) was obtained by measuring around 150 nanofibers, and the histograms' layout was best fitted with the Gauss function.
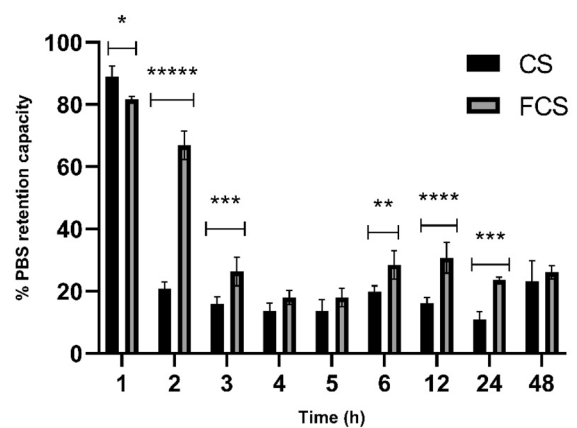
Fig. 5 The PBS retention capacity of CS and FCS over time (*$p < 0.05$, **$p < 0.01$, ***$p < 0.001$, ****$p < 0.0001$, *****$p < 0.00001$) The unpaired t-test—Holm-Šídák revealed significant differences between CS and FCS for 1 h ($p < 0.05$), 2 h ($p < 0.000001$), 3 h ($p < 0.001$), 6 h ($p > 0.01$), 12 h ($p < 0.00001$) and 24 h ($p < 0.0001$)

The SEM analysis for CS showed that the pore diameter (Fig. 4A) ranged from 1.13 to 10.42 μm, and the cellulose fibers size (Fig. 4B) varied from 9 to 114 nm. The highest percentage of cellulose pores was found between the 1.51 and 4.22 μm size having a mean size of 3.66 ± 2.02 μm and for the cellulose fibers size was found a 10–36 nm size range, with the mean size of 25.1 ± 16.8 nm. Thus, the small crystallites led to nanofibers with higher diameters of different values. In the case of FCS, it was observed that the impregnation of the extract produced an increase in pore and fiber sizes compared with the control sample (CS) and ranged from 1.53 to 13.32 μm (Fig. 4C) and from 16 to 163 nm (Fig. 4D), respectively. The highest percentage of cellulose pores was found to be within the 1.95–5.08 μm size range, having a mean size of 4.16 ± 1.97 μm, and for the cellulose fibers size was found a 26–71 nm range, with the mean size 57.9 ± 28.2 nm.

The CS and FCS obtained in this work are comparable to other porous materials obtained from plant (or bacterial) raw materials with similar microscopic features (Liu et al. 2021) and water absorption capacity (Bian et al. 2022). Regarding biological activity, some studies reported absorbent cellulose sponges with similar applications (Paprskářová et al. 2021; Bian et al. 2022), biocompatible aerogels (Zhang

et al. 2023) or as carriers of active principles (Liu et al. 2022).

The spongious material wettability is given by its microscopic characteristics, namely the surface roughness, the surface energy of the materials and the thin surface coatings. Contact angle measurements investigated the hydrophilicity characteristics of the synthesized structures (Supplement Information: video files). The cellulosic spongious materials showed a super hydrophilic behavior (CA ~ 0°), the water droplets being instantly absorbed in the case of FCS, while for the CS, the absorption rate was 1920 ms/μL.

The percentage of PBS absorption was almost similar in case of CS (1463.51%) and FCS (1463.93%) materials, but the absorption capacity is very high, suggesting their usefulness in case of wounds with excess exudate (Abdelrahman and Newton 2011).

Statistically significant differences were observed in terms of fluid retention capacity between CS and FCS (Fig. 5). Thus, for the control, the retention became constant after 2 h, while for the functionalized spongious material the retention was slightly higher, becoming constant after 4 h. The water evaporation rate in the first 4 h was 23.15% evaporated PBS/h for FCS, while for the control, the rate was 68.13% in the first 2 h.

The new spongious material retained a specific humidity when exposed to air in wear conditions for long periods. Thus, these dressings will be advantageous for moderate and high exudate wounds. In addition, water loss could allow uptake of exudates and edema fluid from the dressing through an upward-directed active process, as reported for some commercially available dressings (Kickhöfen et al. 1986; Ngadaonye et al. 2013).

The final materials presented a super hydrophilic surface with a relatively smooth surface that ensures good absorbency and fluid retention. In functionalized spongious material, the slower evaporation of fluids could be explained by hydrogen bonds forming between the mixture of phenols and hydroxyl cellulose groups, which could challenge water evaporation (Fig. 5). The investigated samples show a wicking behavior. In addition, this phenomenon is well-known due to the spontaneous flow of the liquid in a porous substrate, the liquid being driven by the capillary forces. Absorption is the result of natural wetting in a capillary system. The molecular interactions at the interface between a liquid and a solid are based on the physics of wetting and absorption. Quick-drying and wetting are specific phenomena in the processing and use of textiles coming into contact with water or other liquids that the fibrous structures could absorb. These parameters are of the greatest interest in formulating new materials with a degree of comfort and performance of clothing fabrics, hygiene products, medical swabs, etc. (Cotorobai et al. 2016).

To evaluate the release kinetics of the active principles, the total content of phenolic compounds was determined by the Folin–Ciocalteu method and the antioxidant activity was evaluated in temporal dynamics. The releasing profile of active principles varied considerably over time (Fig. 6a), in the first 48 h, the release was linear ($R^2 = 0.9935$) with a velocity of 0.8941 μg GAE/mL xh. Although the active principles migration from the cellulose-based dressings was relatively short, after 48 h, the release of the incorporated extract remains constant. The results were statistically relevant ($p < 0.0001$).

The Folin–Ciocalteu method is an antioxidant assay based on electron transfer, which measures the reductive capacity of an antioxidant (Lamuela-Raventós 2017). The antiradical properties of native cellulose has been previously described (Criado et al. 2015). The cellulose sponge antioxidant activity could be attributed to the presence of the anomeric hydroxyl group, as previously mentioned (Mahmoud et al. 2022). However, the antioxidant effect of cellulose sponge has been much lower compared to pure antioxidants or *P. americana* extract.

In both FRAP (Fig. 6b) and DPPH (Fig. 6c) assays, it was observed that a high concentration of phenolic compounds with antioxidant potential was released in the first release cycle, and then, was reducing overtime.

In the FRAP assay (Fig. 6b), it was observed that in the first 24 h, the highest concentration of antioxidants was released, and a statistically significant difference being observed between FCS and CS after 2 h, 4 h, 24 h ($p < 0.01$) and 12 h ($p < 0.001$).

The antioxidant activity measured by the DPPH assay is inversely proportional to the contact time, with a constant release value maintained after 24 h (Fig. 6c). A statistically significant difference was observed between FCS and CS after 2 h, 4 h, 12 h, 48 h, 72 h ($p < 0.0001$) and 24 h ($p < 0.01$).

Fig. 6 Release capacity of phenolic compounds incorporated in FCS ($p < 0.0001$) (**a**) Antioxidant activity of cellulose functionalized with *P. americana* fruit extract as well as of the cellulose sponge control, by the FRAP assay (**b**) (comparisons between FCS and CS were statistically significant, $p < 0.001$ up to 48 h) and DPPH assay (**c**) (comparisons between FCS and CS were statistically significant, $p < 0.001$)
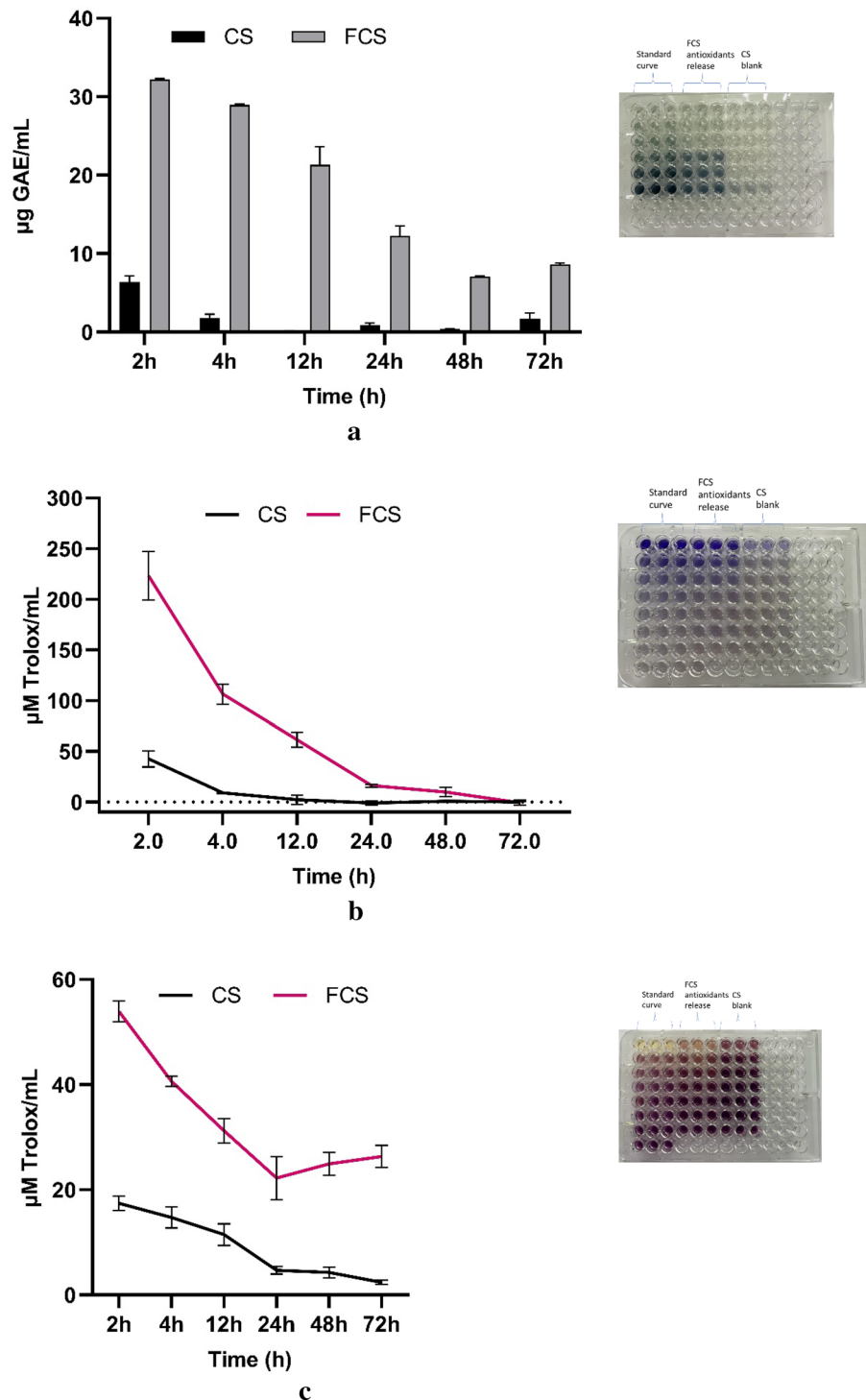
Among the identified compounds, some of them have remarkable antioxidant activity, such as azelaic acid (Sieber and Hegel 2014), isoquercetin (Ma et al. 2018), delphinidin3-O-glucoside (Sari et al. 2019), cyanidin-3-O-glucoside (Olivas-Aguirre et al. 2016), 7-hydroxy-2′,4′,5′-trimethoxyisoflavone, afrormosin
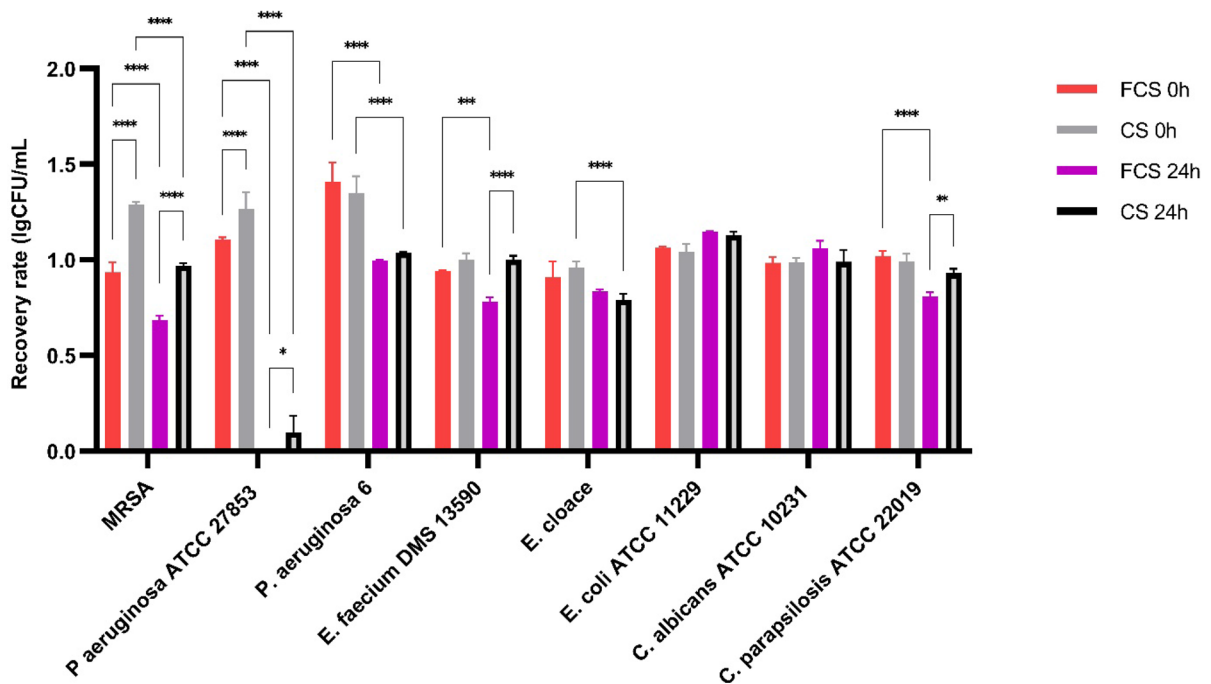
Fig. 7 CFU/mL recovery rate at initial contact time (considered 15 min) and after 24 h incubation at 37 ºC for CS and FCS ($*p < 0.05$, $**p < 0.01$, $***p < 0.001$, $****\ p < 0.0001$)

(Silva et al. 2020), saponarin (Chung et al. 2019), usnic acid (Cetin Cakmak and Gülçin 2019) and medicarpin (Kim et al. 2022).

The release of antioxidant compounds from the bioactive wound dressing could positively impact the healing process by limiting the ROS (Reactive oxygen species) release and, possibly contributing to the occurrence of an antimicrobial effect which will prevent wound infection (Schafer and Werner 2008). In this context, we aimed to study the antioxidant potential and the kinetics of the active compounds release from the functionalized cellulose matrix and further correlated these effects with those of antimicrobial activity assay.

Microbiological control and antimicrobial activity

The degree of contamination showed that sterilization by gamma irradiation using the recommended doses ensured the sterility of the obtained products.

Regarding the antimicrobial activity, the active compounds released from the cellulose matrix inhibited the MRSA strains growth by up to about 30%. A significant difference between CS and FCS was

observed for MRSA ($p < 0.0001$) (Fig. S4), *E. faecium* ($p < 0.0001$), *P. aeruginosa* ATCC ($p < 0.0.5$) (Fig. S5), and *C. parapsilosis* ($p < 0.01$) (Fig. S3) strains (Fig. 7). The growth of *A. baumannii* strain was completely abolished (100%) by both CS and FCS after 15 min (considered 0 h) and 24 h of contact. The calculation of CFU/mL suggested that the functionalized cellulose exhibited a more intense antimicrobial effect as compared to cellulose control.

This antimicrobial activity could be attributed to the presence of: (i) gibberellins, which are known for their antimicrobial properties against phytopathogens and clinical pathogens (Ciucure et al. 2022); (ii) azelaic acid, which is an important moiety for the management of acne, inhibiting the excess follicular sebum and *Propionibacterium acne* growth and exhibiting anti-inflammatory and hyperproliferative activity, according to Kumar et al. (2020); (iii) medicarpin, which has been shown to exhibit anti-gonococcal activity (Williams et al. 2021).

The decrease of CFU/mL induced by CS has been observed in the case of some bacterial strains (*S. aureus, P. aeruginosa,* and *E. cloacae*) in the absence of the active compounds from *P. americana.* This

Fig. 8 The concentration of free hemoglobin expressed as absorbance in the presence of CS and FCS for 50 min of blood clotting
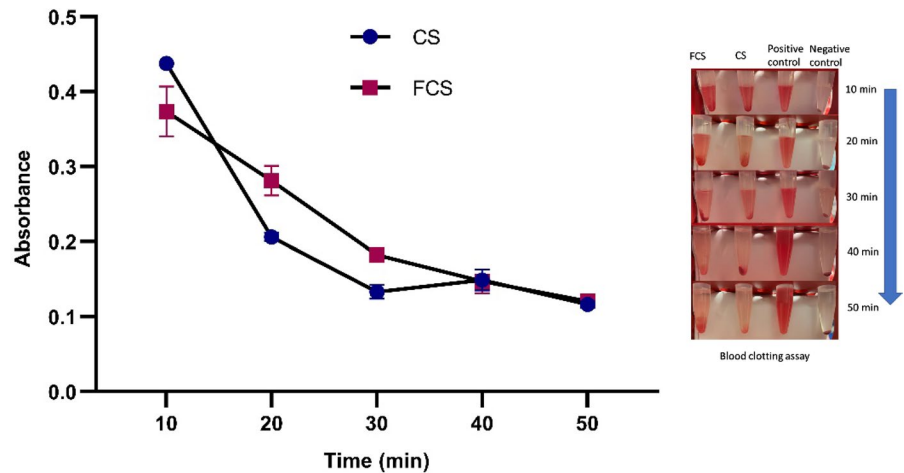
effect could be due to the physical interaction of the spongious material with these bacterial cells, favoring the immobilization of the microbial cells on the material surface, and not necessarily to the presence of a compound with an antimicrobial effect. In exchange, other species, such as *E. coli* (Liu and Yu 2012), *C. albicans* (Chambers et al. 1993) and *C. parapsilosis* (Brexó et al. 2020) were found to produce cellulases that could degrade the cellulose fibers from the sponge material, thus explaining the inconsistency of the CS antibacterial effect for some microbial species. However, in the case of the FCS, cellulase activity could be inhibited by the active principles (the phenolic compounds) from the plant extract (Qin et al. 2016), explaining their antimicrobial effect (Marinas et al. 2021).

Hemocompatibility and biocompatibility

The hemolysis index for CS and FCS was below 5%, i.e., $2.68 \pm 0.29\%$ and $3.28 \pm 0.72\%$, respectively. The presence of saponosides in the FCS conferred to the functionalized cellulose a higher degree of hemolysis, although not statistically significant ($p > 0.05$), compared to the control. Although the complex processes involved in the four phases of wound healing, *i.e.* hemostasis, inflammation, proliferation, and regeneration, have been well characterized histologically, the cellular and molecular pathways that control normal and pathological wound healing are not fully elucidated. It is well known that red blood cells hemolyze in contact with deionized water. Considering the hemolysis rate values obtained for the used

samples, the proposed materials can be classified as medical devices with possible applications as wound dressings for open wounds, for which a hemolysis rate of less than 5% is allowed (Jiang et al. 2011; Reshmi et al. 2018).

The whole blood clotting kinetics is important for evaluating the long-term success of biomaterials in contact with blood. The results indicated that the blood coagulated after 20 min in the case of CS, while for FCS, the blood clotting occurred after 30 min (Fig. 8). The delay in blood clotting may also be due to the slightly higher hemolysis index in the case of FCS. The differences between CS and FCS were not significant after 40 min ($p > 0.05$). However, the difference between CS and FCS was significant statistically after 10 min ($p < 0.05$), 20 min ($p < 0.01$), and 30 min ($p < 0.01$).

Cytotoxicity measured by the LDH assay on the Hep-2 cell line incubated with CS and FCS at different concentrations of 25, 50, 100, 250, and 500 µg/mL is shown in Fig. 9a. The highest biocompatibility was for CS at 100 µg/µL, demonstrated by the increased cell proliferation rates (Fig. 9b, $p < 0.0001$) and similar LDH release with the control ($p > 0.05$). The results are correlated with those provided by the MTT method (Fig. 9b, c). It was observed that the plant extract significantly increases cell proliferation at 100 µg/mL (Fig. 9c, $p < 0.001$) while inhibiting the release of the LDH cytoplasmic enzyme, an indicator of disrupted membrane integrity.

Wound closure is a dynamic mechanical process depending on the proliferation and migration of skin cells. Therefore, the cytocompatibility of novel

a

b

c

d

e
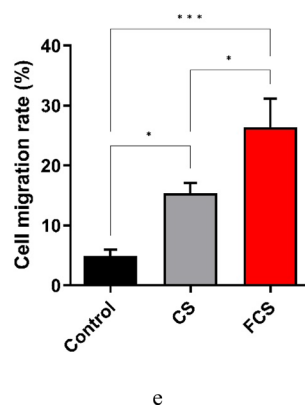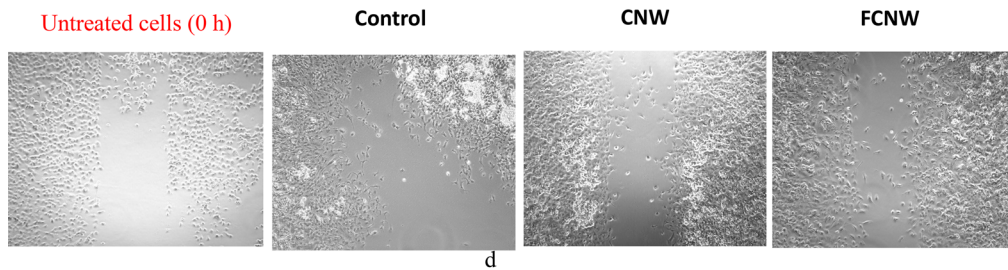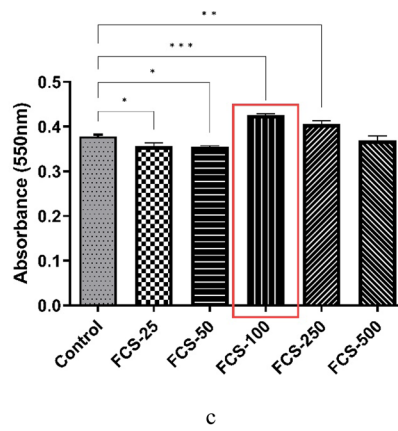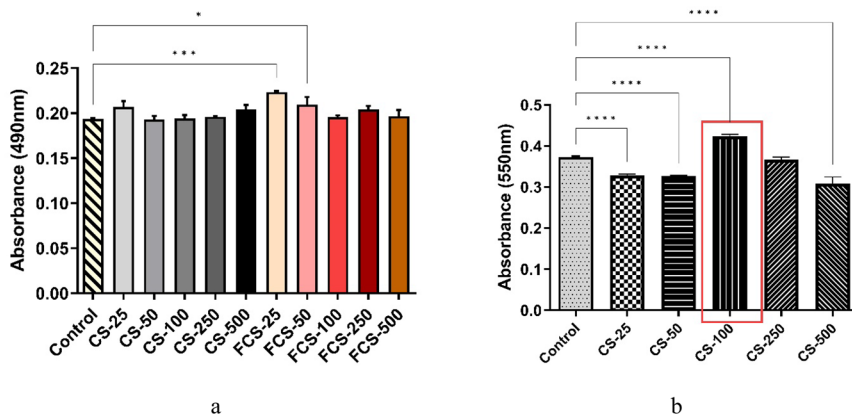
◄**Fig. 9** The comparative biocompatibility of CS vs. FCS: **a** Cell cytotoxicity measured by LDH test—Hep-2 cells co-cultured in the presence of CS and FCS at different concentrations of 25, 50, 100, 250, and 500 µg/mL; **b**, **c** evaluation of cell proliferation and **d**, **e** cell migration. Statistical analysis was performed by reference to the control, represented by cells without any treatment

spongious materials is compulsory to achieve optimal wound healing. The LDH cytotoxicity test provides multiple information on cell viability, allowing the selection of the appropriate concentration for future treatments, which in this case was 100 µg/mL.

Cell migration plays a vital role in wound healing (Muniandy et al. 2018); thus, the monolayer scratch test was performed to observe the extract's influence on cell migration and extrapolate it on wound closure. The wound scratch test is an in vitro assay that mimics the cell migration process during wound healing, and the obtained results demonstrate that the materials positively impact the wound closure process (Agyare et al. 2011; Muniandy et al. 2018) at the optimal concentration that ensures cell viability (100 µg/mL). The values calculated according to the scratch coverage rate reached in 24 h are presented in Fig. 9d.

The migration analysis shows that, for CS, the treated cells showed a significant increase in migration by 15.39% ($p < 0.05$), compared to the control group, which is only 4.9%, while for FCS, cell migration increased to 26.33% ($p < 0.001$). Furthermore,

a significant increase in migration was highlighted by comparing the functionalized spongious material with the non-functionalized one ($p < 0.05$).

A balanced inflammatory response provides the essential factors for wound healing and tissue regeneration during recovery (Eming et al. 2007).

In the present study, the FCS has significantly decreased the production of the pro-inflammatory cytokine IL-6 ($p < 0.01$) and stimulated the production of the anti-inflammatory cytokine IL-10 ($p < 0.001$) in the RAW macrophage cell line, in comparison with CS (Fig. 10a, b). In fact, macrophages' enhanced pro-inflammatory cytokines (such as IL-6) production which can negatively affect tissue repair rate, impairing the normal functions and extracellular matrix production in injured tissues (Eming et al. 2007; Albaayit et al. 2020). On the other part, IL-10 is an anti-inflammatory cytokine produced by several cell types that inhibits IL-1, TNF-α, IL-6, IL-8, and COX-2 production by macrophages, thus protecting cells and tissues from oxidative/nitrosative stress (Figueroa et al. 2015; Albaayit et al. 2016).

The compounds identified in *P. americana* fruit extract responsible for this anti-inflammatory effect are azelaic acid (Sieber and Hegel 2014), isoquercetin (Ma et al. 2018), delphinidin-3-O-glucoside (Sari et al. 2019), cyanidin-3-O-glucoside (Olivas-Aguirre et al. 2016), afrormosin (Ribeiro et al. 2018),

Fig. 10 Effects of the CS and FCS on IL-6 (**a**), and IL-10 (**b**) production in *E. coli*—activated RAW cells at 24 h post-treatment. The results shown in the graphs are mean ± SD. *Means significantly different from those of the *E. coli*—activated RAW control at $p < 0.05$; two-way ANOVA, n = 3

a

b
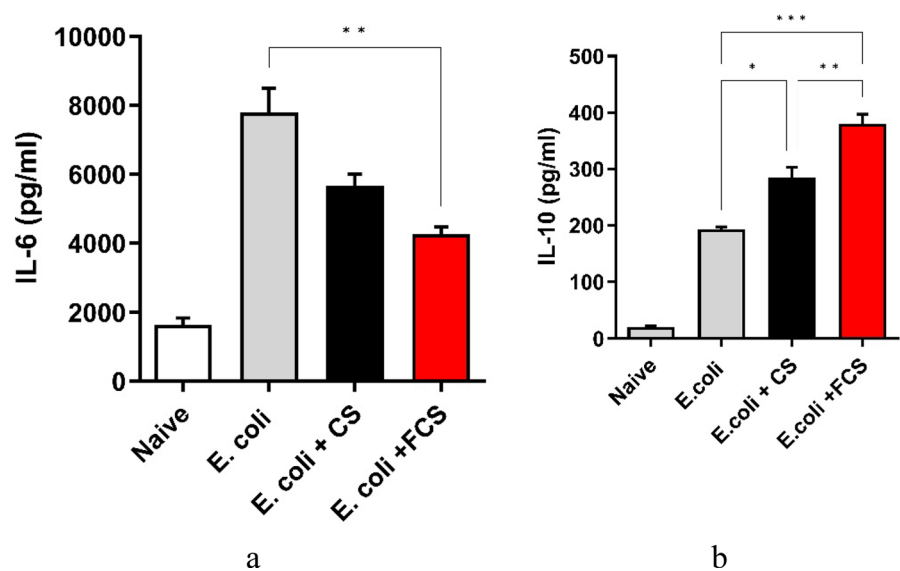
saponarin (Min et al. 2021), usnic acid (Galanty et al. 2021) and [6]-gingerol (Bhaskar et al. 2020).

Other studies have reported the anti-inflammatory activity of some of these compounds. For example, the isoflavonoid afrormosin, isolated from *Amburana cearensis* inhibited neutrophil degranulation and ROS production (Ribeiro et al. 2018). According to Min et al. (2021), saponarin significantly inhibits the degranulation of β-hexosaminidase, phosphorylation of signaling effectors, and the expression of inflammatory mediators (TNF-α, IL-4, IL-5, IL-6, IL-13, COX-2, and FcεRIα/γ) in RBL-2H3 (rat basophilic leukemia) cells stimulated with DNP-IgE and DNP-BSA.

The anti-inflammatory response triggered by the functionalized spongious materials represents a strong argument that they deserve further attention for developing novel bioactive dressings that would facilitate tissue healing and recovery.

Conclusions

The cellulose extracted from *G. triacanthos* pods was purified after ten cycles of delignification. The *P. americana* fruit extract (less toxic and known for the mitogenic effect) used for cellulosic spongious material functionalization had a content of 477.86 ± 6.19 μg TPC (GAE, gallic acid equivalents)/mL extract, with the main compounds identified by UHPLC–ESI–HRMS being cinnamic acid (11,569.41 μg/L), chlorogenic acid (283.65 μg/L), pinostrombin (156.80 μg/L), and vanillic acid (104.28 μg/L). These compounds could promote tissue regeneration by quenching ROS/RNS and reducing NF-κB mediated inflammation (Thangapazham et al. 2016).

The high hydrophilic character of microporous cellulosic sponge from *G. triacanthos* pods functionalized with the *P. americana* fruit extract ensures wound fluids absorption. In addition, the obtained material shows antimicrobial, antioxidant and immunomodulatory properties, which are important for wound healing. Furthermore, the hemolysis rate of less than 5% is within legally acceptable limits. All these results suggest that FCS is an excellent candidate for developing bioactive dressings that could ensure cell proliferation and migration, and simultaneously limit microbial contamination, excessive inflammation, and ROS release. All these effects could increase the skin wounds' healing process. This option also represents a cost-effective and ecological approach to reduce the uncontrolled invasion of non-native plant species and exploit them for novel biomedical applications.

Declarations

Conflict of interests The authors have no financial or non-financial interests to disclose.

Ethics approval and consent to participate Not applicable.

References

Abdelrahman T, Newton H (2011) Wound dressings: principles and practice. Surgery 29:491–495. https://doi.org/10.1016/j.mpsur.2011.06.007

Abe K, Yano H (2009) Comparison of the characteristics of cellulose microfibril aggregates of wood, rice straw and potato tuber. Cellulose 16:1017–1023. https://doi.org/10.1007/s10570-009-9334-9

Agyare C, Lechtenberg M, Deters A et al (2011) Ellagitannins from Phyllanthus muellerianus (Kuntze) Exell.: Geraniin and furosin stimulate cellular activity, differentiation and collagen synthesis of human skin keratinocytes and dermal fibroblasts. Phytomedicine 18:617–624. https://doi.org/10.1016/j.phymed.2010.08.020

Albaayit SFA, Abba Y, Abdullah R, Abdullah N (2016) Prophylactic effects of Clausena excavata Burum. f. leaf extract in ethanol-induced gastric ulcers. Drug Des Devel Ther 10:1973. https://doi.org/10.2147/DDDT.S103993

Albaayit SA, Rasedee A, Abdullah N, Abba Y (2020) Methanolic extract of Clausena excavata promotes wound healing via antiinflammatory and anti-apoptotic activities. Asian Pac J Trop Biomed 10:232. https://doi.org/10.4103/2221-1691.281467

Alexandrescu L, Syverud K, Gatti A, Chinga-Carrasco G (2013) Cytotoxicity tests of cellulose nanofibril-based structures. Cellulose 20:1765–1775. https://doi.org/10.1007/s10570-013-9948-9

Bailly C (2021) Medicinal properties and anti-inflammatory components of Phytolacca (Shanglu). Digit Chin Med 4:159–169. https://doi.org/10.1016/j.dcmed.2021.09.001

Bailly C, Vergoten G (2020) Esculentosides: insights into the potential health benefits, mechanisms of action and molecular targets. Phytomedicine 79:153343. https://doi.org/10.1016/j.phymed.2020.153343

Bajpai SK, Chand N, Ahuja S, Roy MK (2015) Curcumin/cellulose micro crystals/chitosan films: water absorption behavior and in vitro cytotoxicity. Int J Biol Macromol 75:239–247. https://doi.org/10.1016/j.ijbiomac.2015.01.038

Bajpai SK, Ahuja S, Chand N, Bajpai M (2017) Nano cellulose dispersed chitosan film with Ag NPs/Curcumin: an in vivo study on Albino rats for wound dressing. Int J Biol Macromol 104:1012–1019. https://doi.org/10.1016/j.ijbiomac.2017.06.096

Barker BE, Farnes P, LaMarche PH (1966) Peripheral blood plasmacytosis following systemic exposure to Phytolacca americana (pokewood). Pediatrics 38:490–493. https://doi.org/10.1542/peds.38.3.490

Basu A, Heitz K, Strømme M et al (2018) Ion-crosslinked wood-derived nanocellulose hydrogels with tunable antibacterial properties: Candidate materials for advanced wound care applications. Carbohydr Polym 181:345–350. https://doi.org/10.1016/j.carbpol.2017.10.085

Bekeredjian-Ding I, Foermer S, Kirschning CJ et al (2012) Poke weed mitogen requires toll-like receptor ligands for proliferative activity in human and murine B lymphocytes. PLoS One 7:e29806. https://doi.org/10.1371/journal.pone.0029806

Benzie IFF, Strain JJ (1996) The ferric reducing ability of plasma (FRAP) as a measure of "antioxidant power": the FRAP assay. Anal Biochem 239:70–76. https://doi.org/10.1006/abio.1996.0292

Bhaskar A, Kumari A, Singh M et al (2020) [6]-Gingerol exhibits potent anti-mycobacterial and immunomodulatory activity against tuberculosis. Int Immunopharmacol 87:106809. https://doi.org/10.1016/j.intimp.2020.106809

Bian J, Bao L, Gao X et al (2022) Bacteria-engineered porous sponge for hemostasis and vascularization. J Nanobiotechnology 20:47. https://doi.org/10.1186/s12951-022-01254-7

Bodger MP, Mcgiven AR, Fitzgerald PH (1979) Mitogenic proteins of pokeweed I. purification, characterization and mitogenic activity of two proteins from pokeweed (Phytolacca octandra). Immunology 37(4):785

Bordbar S, Anwar F, Saari N (2011) High-value components and bioactives from sea cucumbers for functional foods—a review. Mar Drugs 9:1761–1805. https://doi.org/10.3390/md9101761

Brexó RP, Brandão LR, Chaves RD et al (2020) Yeasts from indigenous culture for cachaça production and brewer's spent grain: biodiversity and phenotypic characterization for biotechnological purposes. Food Bioprod Process 124:107–120. https://doi.org/10.1016/j.fbp.2020.08.006

Cara C, Ruiz E, Ballesteros I et al (2006) Enhanced enzymatic hydrolysis of olive tree wood by steam explosion and alkaline peroxide delignification. Process Biochem 41:423–429. https://doi.org/10.1016/j.procbio.2005.07.007

Carrión-Prieto P, Martín-Ramos P, Hernández-Navarro S et al (2019) Cristalinidad de microfibras de celulosa obtenidas de Cistus ladanifer y Erica arborea. Maderas Cienc y Tecnol 21:447–456. https://doi.org/10.4067/S0718-221X2019005000402

Catalán J, Ilves M, Järventaus H et al (2015) Genotoxic and immunotoxic effects of cellulose nanocrystals in vitro. Environ Mol Mutagen 56:171–182. https://doi.org/10.1002/em.21913

Cetin Cakmak K, Gülçin İ (2019) Anticholinergic and antioxidant activities of usnic acid-an activity-structure insight.

Toxic Rep 6:1273–1280. https://doi.org/10.1016/j.toxrep.2019.11.003

Chambers RS, Walden AR, Brooke GS et al (1993) Identification of a putative active site residue in the exo-β-(1,3)-glucanase of Candida albicans. FEBS Lett 327:366–369. https://doi.org/10.1016/0014-5793(93)81022-R

Chen J, Zhang Y, Guan X et al (2022) Characterization of saponins from differently colored quinoa cultivars and their in vitro gastrointestinal digestion and fermentation properties. J Agric Food Chem 70:1810–1818. https://doi.org/10.1021/acs.jafc.1c06200

Chung N-J, Kim J-Y, Lee Y et al (2019) Variations of saponarin content in young barley leaves illuminated with different light-emitting diodes (LEDs). J Crop Sci Biotechnol 22:317–322. https://doi.org/10.1007/s12892-019-0099-0

Ci X, Zhong W, Ren H et al (2015) Esculentoside A attenuates allergic airway inflammation via activation of the Nrf-2 pathway. Int Arch Allergy Immunol 167:280–290. https://doi.org/10.1159/000441061

Ciucure CT, Geană E (2019) Phenolic compounds profile and biochemical properties of honeys in relationship to the honey floral sources. Phytochem Anal 30:481–492. https://doi.org/10.1002/pca.2831

Ciucure CT, Geana E-I, Sandru C et al (2022) Phytochemical and nutritional profile composition in fruits of different sweet chestnut (Castanea sativa Mill.) cultivars grown in Romania. Separations 9:66. https://doi.org/10.3390/separations9030066

Cotorobai VF, Zgura I, Birzu M et al (2016) Wicking behavior of fabrics described by simultaneous acquiring the images of the wet region and monitoring the liquid weight. Colloids Surf A Physicochem Eng Asp 497:146–153. https://doi.org/10.1016/j.colsurfa.2016.02.040

Criado P, Fraschini C, Salmieri S et al (2015) Evaluation of antioxidant cellulose nanocrystals and applications in gellan gum films. Ind Biotechnol 11:59–68. https://doi.org/10.1089/ind.2014.0017

del Cerro DR, Koso TV, Kakko T et al (2020) Crystallinity reduction and enhancement in the chemical reactivity of cellulose by non-dissolving pre-treatment with tetrabutylphosphonium acetate. Cellulose 27:5545–5562. https://doi.org/10.1007/s10570-020-03044-6

Dhivya S, Padma VV, Santhini E (2015) Wound dressings: a review. Biomedicine 5:22. https://doi.org/10.7603/s40681-015-0022-9

Di Z, Shi Z, Ullah MW et al (2017) A transparent wound dressing based on bacterial cellulose whisker and poly(2-hydroxyethyl methacrylate). Int J Biol Macromol 105:638–644. https://doi.org/10.1016/j.ijbiomac.2017.07.075

Dowsett C, Newton H (2005) Wound bed preparation: TIME in practice. Wounds Uk 1(3):58

Driemeier C (2014) Two-dimensional Rietveld analysis of celluloses from higher plants. Cellulose 21:1065–1073. https://doi.org/10.1007/s10570-013-9995-2

Driemeier C, Calligaris GA (2011) Theoretical and experimental developments for accurate determination of crystallinity of cellulose I materials. J Appl Crystallogr 44:184–192. https://doi.org/10.1107/S0021889810043955

Duchemin B (2017) Size, shape, orientation and crystallinity of cellulose Iβ by X-ray powder diffraction using a free spreadsheet program. Cellulose 24:2727–2741. https://doi.org/10.1007/s10570-017-1318-6

Edelmann A, Diewok J, Schuster KC, Lendl B (2001) Rapid method for the discrimination of red wine cultivars based on mid-infrared spectroscopy of phenolic wine extracts. J Agric Food Chem 49:1139–1145. https://doi.org/10.1021/jf001196p

Eming SA, Krieg T, Davidson JM (2007) Inflammation in wound repair: molecular and cellular mechanisms. J Invest Dermatol 127:514–525. https://doi.org/10.1038/SJ.JID.5700701

Fareez IM, Ibrahim NA, Wan Yaacob WMH et al (2018) Characteristics of cellulose extracted from Josapine pineapple leaf fibre after alkali treatment followed by extensive bleaching. Cellulose 25:4407–4421. https://doi.org/10.1007/s10570-018-1878-0

Farnes P, Barker BE, Brownhill LE, Fanger H (1964) Mitogenic activity in Phytolacca americana (pokeweed). Lancet 284:1100–1101. https://doi.org/10.1016/S0140-6736(64)92616-9

Fernandes EM, Pires RA, Mano JF, Reis RL (2013) Bionanocomposites from lignocellulosic resources: properties, applications and future trends for their use in the biomedical field. Prog Polym Sci 38:1415–1441. https://doi.org/10.1016/j.progpolymsci.2013.05.013

Fernández K, Agosin E (2007) Quantitative analysis of red wine tannins using Fourier-transform mid-infrared spectrometry. J Agric Food Chem 55:7294–7300. https://doi.org/10.1021/jf071193d

Figueroa LA, Navarro LB, Patiño Vera M, Petricevich VL (2015) Preliminary studies of the immunomodulator effect of the Bougainvillea xbuttiana extract in a mouse model. Evidence-Based Complement Altern Med. https://doi.org/10.1155/2015/479412

French AD (2014) Idealized powder diffraction patterns for cellulose polymorphs. Cellulose 21:885–896. https://doi.org/10.1007/s10570-013-0030-4

French AD (2020) Increment in evolution of cellulose crystallinity analysis. Cellulose 27:5445–5448. https://doi.org/10.1007/s10570-020-03172-z

Galanty A, Zagrodzki P, Gdula-Argasí Nska J et al (2021) A comparative survey of anti-melanoma and anti-inflammatory potential of usnic acid enantiomers-a comprehensive in vitro approach. Pharmaceuticals. https://doi.org/10.3390/ph14090945

Garside P, Wyeth P (2003) Identification of cellulosic fibres by FTIR spectroscopy-thread and single fibre analysis by attenuated total reflectance. Stud Conserv 48:269–275. https://doi.org/10.1179/sic.2003.48.4.269

Gaur R, Azizi M, Gan J et al (2009) British pharmacopoeia, 6th edn. London, 9983

Gawryla MD, van den Berg O, Weder C, Schiraldi DA (2009) Clay aerogel/cellulose whisker nanocomposites: a nanoscale wattle and daub. J Mater Chem 19:2118. https://doi.org/10.1039/b823218k

Gomes PB, Noronha EC, de Melo CTV et al (2008) Central effects of isolated fractions from the root of Petiveria alliacea L. (tipi) in mice. J Ethnopharmacol 120:209–214. https://doi.org/10.1016/j.jep.2008.08.012

Gümüskaya E, Usta M, Kirci H (2003) The effects of various pulping conditions on crystalline structure of cellulose in

cotton linters. Polym Degrad Stab 81:559–564. https://doi.org/10.1016/S0141-3910(03)00157-5

Gustaite S, Kazlauske J, Bobokalonov J et al (2015) Characterization of cellulose based sponges for wound dressings. Colloids Surf A Physicochem Eng Asp 480:336–342. https://doi.org/10.1016/j.colsurfa.2014.08.022

Hajimohammadi R, Hosseini M, Amani H, Najafpour GD (2016) Production of saponin biosurfactant from Glycyrrhiza glabra as an agent for upgrading heavy crude oil. J Surfactants Deterg 19:1251–1261. https://doi.org/10.1007/s11743-016-1871-2

Hamissou M, Kurdmongkoltham P (2015) Molecular and cytotoxicity investigations of Phytolacca americana (1.) root, leaf, and berry extracts. Int J Pharmacol Toxicol 3:11. https://doi.org/10.14419/ijpt.v3i2.5160

Han S, Sun Q, Zheng H et al (2016) Green and facile fabrication of carbon aerogels from cellulose-based waste newspaper for solving organic pollution. Carbohydr Polym 136:95–100. https://doi.org/10.1016/j.carbpol.2015.09.024

Hohrenk LL, Itzel F, Baetz N et al (2020) Comparison of software tools for liquid chromatography–high-resolution mass spectrometry data processing in nontarget screening of environmental samples. Anal Chem 92:1898–1907. https://doi.org/10.1021/acs.analchem.9b04095

Holloran P (2006) Measuring performance of invasive plant eradication efforts in New Zealand. New Zeal Plant Prot 59:1–7. https://doi.org/10.30843/nzpp.2006.59.4489

Jeong M-J, Lee S, Kang K-Y, Potthast A (2015) Changes in the structure of cellulose aerogels with depolymerization. J Korean Phys Soc 67:742–745. https://doi.org/10.3938/jkps.67.742

Jianan C, Shaoqiong Y, Jinyue R (1996) A study on the preparation, structure, and properties of microcrystalline cellulose. J Macromol Sci Part A 33:1851–1862. https://doi.org/10.1080/10601329608011011

Jiang H, Wang XB, Li CY et al (2011) Improvement of hemocompatibility of polycaprolactone film surfaces with zwitterionic polymer brushes. Langmuir 27:11575–11581. https://doi.org/10.1021/la202101q

Kickhöfen B, Wokalek H, Scheel D, Ruh H (1986) Chemical and physical properties of a hydrogel wound dressing. Biomaterials 7:67–72. https://doi.org/10.1016/0142-9612(86)90092-X

Kim J-H, Kang D-M, Cho Y-J et al (2022) Medicarpin increases antioxidant genes by inducing NRF2 transcriptional level in HeLa cells. Antioxidants 11:421. https://doi.org/10.3390/antiox11020421

Kumar A, Rao R, Yadav P (2020) Azelaic acid: a promising agent for dermatological applications. Curr Drug Ther 15:181–193. https://doi.org/10.2174/1574885514666190904160228

Kumar Rai P, Singh JS (2020) Invasive alien plant species: their impact on environment, ecosystem services and human health. Ecol Indic 111:106020. https://doi.org/10.1016/j.ecolind.2019.106020

Laghi L, Versari A, Parpinello GP et al (2011) FTIR spectroscopy and direct orthogonal signal correction preprocessing applied to selected phenolic compounds in red wines. Food Anal Methods 4:619–625. https://doi.org/10.1007/s12161-011-9240-2

Lamuela-Raventós RM (2017) Folin–Ciocalteu method for the measurement of total phenolic content and antioxidant capacity. Measurement of antioxidant activity & capacity. Wiley, Chichester, pp 107–115

Lee S, Jeong M-J, Kang K-Y (2015) Preparation of cellulose aerogels as a nano-biomaterial from lignocellulosic biomass. J Korean Phys Soc 67:738–741. https://doi.org/10.3938/jkps.67.738

Lin L, Peng S, Shi C et al (2022) Preparation and characterization of cassava starch/sodium carboxymethyl cellulose edible film incorporating apple polyphenols. Int J Biol Macromol 212:155–164. https://doi.org/10.1016/j.ijbiomac.2022.05.121

Liu M, Yu H (2012) Co-production of a whole cellulase system in Escherichia coli. Biochem Eng J 69:204–210. https://doi.org/10.1016/j.bej.2012.09.011

Liu C, Yu J, You J et al (2021) Cellulose/chitosan composite sponge for efficient protein adsorption. Ind Eng Chem Res 60:9159–9166. https://doi.org/10.1021/acs.iecr.1c01133

Liu E-J, Huang J-X, Hu R-Z et al (2022) A hierarchical porous cellulose sponge modified with chlorogenic acid as a antibacterial material for water disinfection. Sustainability 15:773. https://doi.org/10.3390/su15010773

Long L-Y, Weng Y-X, Wang Y-Z (2018) Cellulose aerogels: synthesis, applications, and prospects. Polymers (Basel) 10:623. https://doi.org/10.3390/polym10060623

Lu B, Wang T, Li Z et al (2016) Healing of skin wounds with a chitosan–gelatin sponge loaded with tannins and platelet-rich plasma. Int J Biol Macromol 82:884–891. https://doi.org/10.1016/j.ijbiomac.2015.11.009

Ma C, Jiang Y, Zhang X et al (2018) Isoquercetin ameliorates myocardial infarction through anti-inflammation and anti-apoptosis factor and regulating TLR4-NF-κB signal pathway. Mol Med Rep. https://doi.org/10.3892/mmr.2018.8709

Madhu G, Bose VC, Aiswaryaraj AS et al (2013) Defect dependent antioxidant activity of nanostructured nickel oxide synthesized through a novel chemical method. Colloids Surf A Physicochem Eng Asp 429:44–50. https://doi.org/10.1016/j.colsurfa.2013.03.055

Mahdavi M, Mahmoudi N, Rezaie Anaran F, Simchi A (2016) Electrospinning of nanodiamond-modified polysaccharide nanofibers with physico-mechanical properties close to natural skins. Mar Drugs 14:128. https://doi.org/10.3390/md14070128

Mahmoud S, Ali S, Omar A (2022) Nano cellulose as sustainable green material for multi biological applications via ξ potential. Res Sq. https://doi.org/10.21203/rs.3.rs-1755008/v1

Marinas IC, Oprea E, Geana E-I et al (2020) Valorization of Gleditsia triacanthos invasive plant cellulose microfibers and phenolic compounds for obtaining multi-functional wound dressings with antimicrobial and antioxidant properties. Int J Mol Sci Artic. https://doi.org/10.3390/ijms22010033

Marinas IC, Oprea E, Geana EI (2021) Chemical composition, antimicrobial and antioxidant activity of Phytolacca americana L. fruits and leaves extracts. Farmacia 69:883–889. https://doi.org/10.31925/farmacia.2021.5.9

Martínez Ávila H, Schwarz S, Feldmann E-M et al (2014) Biocompatibility evaluation of densified

bacterial nanocellulose hydrogel as an implant material for auricular cartilage regeneration. Appl Microbiol Biotechnol 98:7423–7435. https://doi.org/10.1007/s00253-014-5819-z

Min SY, Park CH, Yu HW, Park YJ (2021) Anti-inflammatory and anti-allergic effects of saponarin and its impact on signaling pathways of RAW 264.7, RBL-2H3, and HaCaT cells. Int J Mol Sci 22(16):8431. https://doi.org/10.3390/IJMS22168431

Moon RJ, Martini A, Nairn J et al (2011) Cellulose nanomaterials review: structure, properties and nanocomposites. Chem Soc Rev 40:3941. https://doi.org/10.1039/c0cs00108b

Muniandy K, Gothai S, Tan WS et al (2018) In vitro wound healing potential of stem extract of *Alternanthera sessilis*. Evidence-Based Complement Altern Med 2018:1–13. https://doi.org/10.1155/2018/3142073

Naseri-Nosar M, Ziora ZM (2018) Wound dressings from naturally-occurring polymers: a review on homopolysaccharide-based composites. Carbohydr Polym 189:379–398. https://doi.org/10.1016/j.carbpol.2018.02.003

Ngadaonye JI, Geever LM, Killion J, Higginbotham CL (2013) Development of novel chitosan-poly(N, N-diethylacrylamide) IPN films for potential wound dressing and biomedical applications. J Polym Res 20:161. https://doi.org/10.1007/s10965-013-0161-1

Nie J, Wu Z, Pang B et al (2022) Fabrication of ZnO@Plant polyphenols/cellulose as active food packaging and its enhanced antibacterial activity. Int J Mol Sci 23:5218. https://doi.org/10.3390/ijms23095218

Nishiyama Y, Langan P, Chanzy H (2002) Crystal structure and hydrogen-bonding system in cellulose iβ from synchrotron X-ray and neutron fiber diffraction. J Am Chem Soc 124:9074–9082. https://doi.org/10.1021/ja0257319

Olivas-Aguirre F, Rodrigo-García J, Martínez-Ruiz N et al (2016) Cyanidin-3-O-glucoside: physical-chemistry foodomics and health effects. Molecules 21:1264. https://doi.org/10.3390/molecules21091264

Ong SY, Wu J, Moochhala SM et al (2008) Development of a chitosan-based wound dressing with improved hemostatic and antimicrobial properties. Biomaterials 29:4323–4332. https://doi.org/10.1016/j.biomaterials.2008.07.034

Paprskářová A, Suchý P, Chalupová M et al (2021) Evaluation and comparison of structurally different cellulose-based hemostatic agents in a rat kidney model. Cellulose 28:9369–9382. https://doi.org/10.1007/s10570-021-04104-1

Patra JK, Kim ES, Oh K et al (2014) Antibacterial effect of crude extract and metabolites of Phytolacca americana on pathogens responsible for periodontal inflammatory diseases and dental caries. BMC Complement Altern Med 14:343. https://doi.org/10.1186/1472-6882-14-343

Patterson AL (1939) The diffraction of X-rays by small crystalline particles. Phys Rev 56:972–977. https://doi.org/10.1103/PhysRev.56.972

Pecharsky VK, Zavalij PY (2008) Fundamentals of powder diffraction and structural characterization of materials. XXIV:744. https://doi.org/10.1007/978-0-387-09579-0

Phirom-on K, Apiraksakorn J (2022) Eco-friendly extraction of banana peel cellulose using a wood charcoal ash solution and application of process wastewater as

a naturally-derived product. Bioresour Technol Rep 19:101174. https://doi.org/10.1016/j.biteb.2022.101174

Poletto M, Pistor V, Ademir J (2013) Structural characteristics and thermal properties of native cellulose. In: van de Ven T, Godbout L (eds) Cellulose-fundamental aspects. InTech, p 378

Qin L, Li W-C, Liu L et al (2016) Inhibition of lignin-derived phenolic compounds to cellulase. Biotechnol Biofuels 9:70. https://doi.org/10.1186/s13068-016-0485-2

Qin Y, Xu F, Yuan L et al (2020) Comparison of the physical and functional properties of starch/polyvinyl alcohol films containing anthocyanins and/or betacyanins. Int J Biol Macromol 163:898–909. https://doi.org/10.1016/j.ijbiomac.2020.07.065

Rathi N, Paradkar A, Gaikar VG (2019) Polymorphs of curcumin and its cocrystals with cinnamic acid. J Pharm Sci 108:2505–2516. https://doi.org/10.1016/j.xphs.2019.03.014

Ravikiran G, Raju A, Venugopal Y (2011) Phytolacca americana: a review. Int J Res Pharma Biomed Sci 2:942–946

Reddy N, Yang Y (2009) Properties and potential applications of natural cellulose fibers from the bark of cotton stalks. Bioresour Technol 100:3563–3569. https://doi.org/10.1016/j.biortech.2009.02.047

Rees A, Powell LC, Chinga-Carrasco G et al (2015) 3D bioprinting of carboxymethylated-periodate oxidized nanocellulose constructs for wound dressing applications. Biomed Res Int 2015:1–7. https://doi.org/10.1155/2015/925757

Reshmi C, Suja P, Manaf O et al (2018) Nanochitosan enriched poly ε-caprolactone electrospun wound dressing membranes: A fine tuning of physicochemical properties, hemocompatibility and curcumin release profile. Int J Biol Macromol 108:1261–1272. https://doi.org/10.1016/j.ijbiomac.2017.11.035

Ribeiro VP, Arruda C, El-Salam MA, Bastos JK (2018) Brazilian medicinal plants with corroborated anti-inflammatory activities: a review. Pharm Biol 56:253–268. https://doi.org/10.1080/13880209.2018.1454480

Rietveld HM (1967) Line profiles of neutron powder-diffraction peaks for structure refinement. Acta Crystallogr 22:151–152. https://doi.org/10.1107/S0365110X67000234

Rietveld HM (1969) A profile refinement method for nuclear and magnetic structures. J Appl Crystallogr 2:65–71. https://doi.org/10.1107/S0021889869006558

Saleri F, Chen G, Li X, Guo M (2017) Comparative analysis of saponins from different Phytolaccaceae species and their antiproliferative activities. Molecules 22:1077. https://doi.org/10.3390/molecules22071077

Sari D, Cairns J, Safitri A, Fatchiyah F (2019) Virtual prediction of the delphinidin-3-o-glucoside and peonidin-3-o-glucoside as anti-inflammatory of TNF- and #945. Signal Acta Inform Medica 27:152. https://doi.org/10.5455/aim.2019.27.152-157

Schafer M, Werner S (2008) Oxidative stress in normal and impaired wound repair. Pharmacol Res 58:165–171. https://doi.org/10.1016/j.phrs.2008.06.004

Segal L, Creely JJ, Martin AE, Conrad CM (1959) An empirical method for estimating the degree of crystallinity of native cellulose using the X-ray diffractometer. Text Res

J 29:786–794. https://doi.org/10.1177/004051755902901003

Serbezeanu D, Vlad-Bubulac T, Rusu D et al (2019) Functional polyimide-based electrospun fibers for biomedical application. Materials (basel) 12:3201. https://doi.org/10.3390/ma12193201

Shao X, Sun H, Jiang R, Yu Y (2020) Physical and antibacterial properties of corn distarch phosphate/carboxymethyl cellulose composite films containing tea polyphenol. J Food Process Preserv. https://doi.org/10.1111/jfpp.14401

Shedoeva A, Leavesley D, Upton Z, Fan C (2019) Wound healing and the use of medicinal plants. Evidence-Based Complement Altern Med 2019:1–30. https://doi.org/10.1155/2019/2684108

Sieber MA, Hegel JKE (2014) Azelaic acid: properties and mode of action. Skin Pharmacol Physiol 27:9–17. https://doi.org/10.1159/000354888

Silva JHC, Ferreira RS, Pereira EP et al (2020) Amburana cearensis: pharmacological and neuroprotective effects of its compounds. Molecules 25:3394. https://doi.org/10.3390/molecules25153394

Singleton V, Rossi J (1965) Colorimetry of total phenolics with phosphomolybdic-phosphotungstic acid reagents. Am J Enol Vitic 16:144–158

Siqueira G, Bras J, Dufresne A (2010) Cellulosic bionanocomposites: a review of preparation, properties and applications. Polymers (basel) 2:728–765. https://doi.org/10.3390/polym2040728

Smith BS, Yoriya S, Grissom L et al (2010) Hemocompatibility of titania nanotube arrays. J Biomed Mater Res Part A 95A:350–360. https://doi.org/10.1002/jbm.a.32853

Souza SF, Mariano M, Reis D et al (2018) Cell interactions and cytotoxic studies of cellulose nanofibers from Curauá natural fibers. Carbohydr Polym 201:87–95. https://doi.org/10.1016/j.carbpol.2018.08.056

SR EN ISO 11737-1 (2006) Sterilization of medical devices—microbiological methods—Part 1: determination of a population of microorganisms on products

Stan GE, Tite T, Popa A-C et al (2020) The beneficial mechanical and biological outcomes of thin copper-gallium doped silica-rich bio-active glass implant-type coatings. Coatings 10:1119. https://doi.org/10.3390/coatings10111119

Takumi-Tanimukai Y, Yamamoto S, Ogasawara N et al (2022) A hydroxypropyl methylcellulose plaque assay for human respiratory syncytial virus. J Virol Methods 304:114528. https://doi.org/10.1016/j.jviromet.2022.114528

Thaipong K, Boonprakob U, Crosby K et al (2006) Comparison of ABTS, DPPH, FRAP, and ORAC assays for estimating antioxidant activity from guava fruit extracts. J Food Compos Anal 19:669–675. https://doi.org/10.1016/j.jfca.2006.01.003

Thangapazham RL, Sharad S, Maheshwari RK (2016) Phytochemicals in wound healing. Adv Wound Care 5:230–241. https://doi.org/10.1089/wound.2013.0505

Thygesen A, Oddershede J, Lilholt H et al (2005) On the determination of crystallinity and cellulose content in plant fibres. Cellulose 12:563–576. https://doi.org/10.1007/s10570-005-9001-8

Trache D, Hussin MH, Hui Chuin CT et al (2016) Microcrystalline cellulose: isolation, characterization and bio-composites application: a review. Int J Biol Macromol 93:789–804. https://doi.org/10.1016/j.ijbiomac.2016.09.056

Vartiainen J, Pöhler T, Sirola K et al (2011) Health and environmental safety aspects of friction grinding and spray drying of microfibrillated cellulose. Cellulose 18:775–786. https://doi.org/10.1007/s10570-011-9501-7

Virtanen T, Svedström K, Andersson S et al (2012) A physicochemical characterisation of new raw materials for microcrystalline cellulose manufacturing. Cellulose 19:219–235. https://doi.org/10.1007/s10570-011-9636-6

Wei F, Singh RSP, Fueth M et al (2015) Development and validation of a HPLC–MS/MS method for the determination of phytolaccagenin in rat plasma and application to a pharmacokinetic study. J Pharm Biomed Anal 107:82–88. https://doi.org/10.1016/j.jpba.2014.12.025

Williams D, Perry D, Carraway J et al (2021) Antigonococcal activity of (+)-medicarpin. ACS Omega 6:15274–15278. https://doi.org/10.1021/acsomega.1c01590

Yao W, Weng Y, Catchmark JM (2020) Improved cellulose X-ray diffraction analysis using Fourier series modeling. Cellulose 27:5563–5579. https://doi.org/10.1007/s10570-020-03177-8

Ye D, Zhong Z, Xu H et al (2016) Construction of cellulose/nanosilver sponge materials and their antibacterial activities for infected wounds healing. Cellulose 23:749–763. https://doi.org/10.1007/s10570-015-0851-4

Zeng M-S, Yu W-D, Wang H-X et al (2021) A potential antiviral activity of Esculentoside A against binding interactions of SARS-COV-2 spike protein and angiotensin converting enzyme 2 (ACE2). Int J Biol Macromol 183:2248–2261. https://doi.org/10.1016/j.ijbiomac.2021.06.017

Zhang M, Guo N, Sun Y et al (2023) Nanocellulose aerogels from banana pseudo-stem as a wound dressing. Ind Crops Prod 194:116383. https://doi.org/10.1016/j.indcrop.2023.116383

Zhao Y, Gao G, Liu D et al (2017) Vapor sensing with color-tunable multilayered coatings of cellulose nanocrystals. Carbohydr Polym 174:39–47. https://doi.org/10.1016/j.carbpol.2017.06.059

Zhuo X, Liu C, Pan R et al (2017) Nanocellulose mechanically isolated from Amorpha fruticosa Linn. ACS Sustain Chem Eng 5:4414–4420. https://doi.org/10.1021/acssuschemeng.7b00478

Rigaku Corporation. Rietveld Analysis, *https://www.rigaku.com/techniques/rietveld-analysis*, 2.8.4.0., https://www.rigaku.com/techniques/rietveld-analysis (2018).